Florida International University
FIU Digital Commons

FIU Electronic Theses and Dissertations | University Graduate School

12-2-2011

Evaluation of Wind Loads on Solar Panels

Johann Barata
Florida International University, jbara005@fiu.edu

DOI: 10.25148/etd.FI12041903
Follow this and additional works at: https://digitalcommons.fiu.edu/etd

Recommended Citation
Barata, Johann, "Evaluation of Wind Loads on Solar Panels" (2011). *FIU Electronic Theses and Dissertations*. 567.
https://digitalcommons.fiu.edu/etd/567

This work is brought to you for free and open access by the University Graduate School at FIU Digital Commons. It has been accepted for inclusion in FIU Electronic Theses and Dissertations by an authorized administrator of FIU Digital Commons. For more information, please contact dcc@fiu.edu.

FLORIDA INTERNATIONAL UNIVERSITY

Miami, Florida

EVALUATION OF WIND LOADS IN SOLAR PANELS

A thesis submitted in partial fulfillment of

the requirements for the degree of

MASTER OF SCIENCE

in

CIVIL ENGINEERING

by

Johann Barata

2012

To: Dean Amir Mirmiran
College of Engineering and Computing

This thesis, written by Johann Barata, and entitled Evaluation of Wind loads on Solar panels, having been approved in respect to style and intellectual content, is referred to you for judgment.

We have read this thesis and recommend that it be approved.

_____
Arindam Gan Chowdhury

_____
Yimin Zhu

_____
Girma Bitsuamlak, Major Professor

Date of Defense: December 2, 2011

The thesis of Johann Barata is approved.

_____
Dean Amir Mirmiran
College of Engineering and Computing

_____
Dean Lakshmi N. Reddi
University Graduate School

Florida International University, 2012

DEDICATION

I dedicate this thesis to my son Jonathan G. Barata, to my wife Danay Barata, and to my professor Dr. Girma Bitsuamlak. They all gave the courage and motivation to make this research a reality. I am truly grateful to all of you.

ACKNOWLEDGMENTS

I would like to thank my professor, Dr. Girma Tsegaye Bitsuamlak, who gave me a thorough guidance to complete this thesis work, and for inspiring me to work with Wind Engineering as part of the Master of Science in Civil Engineering program at Florida International University. I would also like to thank Dr. Arindam Gan Chowdhury and Dr. Yimin Zhu for their assistance in the completion of this work.

My thesis would not have been possible without the support of my friends; Amanuel Tecle, who was particularly helpful in guiding me towards the various steps of this project, Workamaw P. Warsido who made it possible by doing the statistical analysis of the data, the *"Wall of Wind"* researchers, and the staff of the RWDI for their support especially Marco Arccado and Bruce McInnis. I will also like to thank my friend and colleague Christian A. Vidal, who dedicatedly proofread my work and suggested modifications. I am also grateful to all my peers and the people who made my time in school an amazing experience.

ABSTRACT OF THE THESIS

EVALUATION OF WIND LOADS ON SOLAR PANELS

by

Johnn Barata

Florida International University, 2012

Miami, Florida

Professor Dr. Girma Tsegaye Bitsuamlak, Major Professor

The current impetus for alternative energy sources is increasing the demand for solar energy technologies in Florida – the Sunshine State. Florida's energy production from solar, thermal or photovoltaic sources accounts for only 0.005% of the state total energy generation. The existing types of technologies, methods of installation, and mounting locations for solar panels vary significantly, and are consequently affected by wind loads in different ways. The fact that Florida is frequently under hurricane risk and the lack of information related with design wind loads on solar panels result in a limited use of solar panels for generating energy in the "Sunshine State" Florida. By using Boundary Layer Wind Tunnel testing techniques, the present study evaluates the effects of wind on solar panels, and provides explicit and reliable information on design wind loads in the form of pressure coefficient value. The study considered two different types of solar panel arrangements, (1) isolated solar panel and (2) arrays, and two different mounting locations, (1) ground mounted and (2) roof mounted. Detailed wind load information was produced as part of this study for isolated and arrayed solar panels. Two main conclusions from this study are the

following:(1) for isolated solar panel with high slopes the wind load for wind angle of attack (AoA) perpendicular to the main axis exhibited the largest wind loads; (2) for arrays, while the outer rows and column were subjected to high wind loads for AoA perpendicular to the main axis, the interior solar panels were subjected to higher loads for oblique AoA.

TABLE OF CONTENTS

CHAPTER PAGE

1. INTRODUCTION 1

2.RESEARH HYPOTHESIS 2

3. RESEARCH OBJECTIVE 2

4.LITERATURE REVIEW 3

5.METHODOLOGY 7
5.1. Boundary layer wind tunnel setup and flow characteristics. 7
5.2. Isolated solar panel: study wind tunnel model and instrumentation. 9
5.3. Solar Panel Array: Wind Tunnel Study Model and Instrumentation 13
5.3.1. Ground-Mounted Arrayed Solar Panel: 13
5.4. Roof-mounted arrayed solar panel 21

6. RESULTS AND DISCUSSIONS 27
6.1. Wind pressure coefficient. 27
6.2. Single Ground Mounted Solar Panel 28
6.2.1. Variation of wind pressure coefficients with wind angle of attack (AoA) 28
6.2.2. Effects of support heights (H) on wind pressure coefficients 32
6.2.3. Effects of Solar Panel Slope (S10, 20, 25, 30 And 40) On Wind Pressure Coefficients 34
6.2.4. Effects of upstream exposure (open vs. suburban) on wind pressure coefficients 36
6.3. Solar panel array: study wind tunnel model and instrumentation 36
6.3.1. Ground- mounted solar pane array 37
6.3.1.1. Variation of wind pressure coefficients with wind angle of attack (AOA) 37
6.3.1.2. Effects of longitudinal distance between the arrays on Cp values 41
6.3.1.3. Effects of Lateral gap between the solar panel on Cp values 45
6.3.2. Roof Mounted solar panels array 51
6.3.2.1. Variation of wind pressure coefficients with wind angle of attack (AoA) 51
6.3.2.2. Effects of roof perimeter gap on Cp values 53

CONCLUSIONS AND RECOMMENDATIONS 63

REFERENCES 65

TABLE OF FIGURES

FIGURE PAGE

Figure 1. Trapezoidal planks and triangular floor roughness elements used to develop open exposure for the bottom 30 m, mean wind speed profile, turbulence intensity profile, and longitudinal turbulence spectrum at 3.81cm (1.5in) height in the mode 8

Figure 2. Isolated solar panel model in a boundary layer wind tunnel in a testing position. 9

Figure 3. Isolated solar panel slopes and support heights considered in the study..... 11

Figure 4.Pressure tap distribution used for Single PV model. 12

Figure 5. Ground-mounted arrayed solar panel model in a boundary layer wind tunnel in a testing position. 14

Figure 6.Pressure tap distribution used for both ground- and roof-mounted model. Note: For arrayed case a total of ten PV panels were instrumented simultaneously with this tap distribution for each test case. 15

Figure 7.Ground-mounted solar panel: Longitudinal distances investigated in the wind tunnel. 16

Figure 8.Ground-mounted solar panels: Lateral gaps..... 17

Figure 9.Ground-mounted arrays considered in the present study..... 18

Figure 10.Ground-mounted array test configuration definition. 19

Figure 11.Roof-mounted arrayed solar panel model in a boundary layer wind tunnel in a testing position. 22

Figure 12.Roof-mounted arrays basic test configuration definition. 23

Figure 13.Perimeter gaps considered for roof-mounted solar panel array. 24

Figure 14.Total roof-mounted array test configurations..... 25

Figure 15.Wind profile, and reference height definition. 27

Figure 16.Maximum Cp Plots for (a) 0^{o} (b) 45 ^{o} (c) 90 ^{o} (d) 135^{0} (e) 180^{0} (f) 225^{0} (g) 270 ^{o}, and (h) 315^{o} wind AoAs. 30

Figure 17.Minimum Cp Plots for (a) 0^{o} (b) 45 ^{o} (c) 90 ^{o} (d) 135^{0} (e) 180^{0} (f) 225^{0} (g) 270 ^{o}, and (h) 315^{o} wind AoAs. 32

Figure 18.(a) Mean Cp for H12, H24, and H32 and wind AoA 1800 and (b) maximum Cp for H12, H24, and H32 and wind AoA 1800. 33

Figure 19.(a) Mean Cp for H12, H24, and H32 and wind AoA 45^0 and (b) Maximum Cp for H12, H24, and H32 and wind AoA 45^0. 34

Figure 20.(a) Mean Cp for S10, S20, S25, S30 and S40 and wind AoA 180^0 (open terrain), and (b)Maximum Cp for S10, S20, S25, S30 and S40 and wind AoA 180^0 (open terrain). 35

Figure 21.(a) Mean Cp for S10, S20, S25, S30 and S40 and wind AoA 45^0(open terrain) and (b) maximum Cp for S10, S20, S25, S30 and S40 and wind AoA 45^0. 35

Figure 22.. Variation of the average CP for different open and suburban profiles (a) 45^0 and (b) 180^0 AoA. 36

Figure 23.Net Cp contours for wind AOAs (a) 00 (b) 315^0, (c) 225^0 and (d) 180^0. 41

Figure 24. Ground-mounted arrays: net Cp contours for longitudinal gap (a) 24 in, (b) 48 in and (c) 72 and AoA 0^0. 41

Figure 25. Ground-mounted arrays: Net Cp contours for longitudinal gap (a) 24 in, (b) 48 in and (c) 72 and AoA 3150.. 41

Figure 26. Ground-mounted arrays: Net Cp contours for longitudinal gap (a) 24 in, (b) 48 in and (c) 72 and AoA 1800.. 41

Figure 27. Ground-mounted array: net Cp contours for longitudinal gap (a) 24 in, (b) 48 in and (c) 72 and AoA 2150.. 41

Figure 28. Ground-mounted array: net Cp contours for lateral gap (a) 0 in, (b) 32 in and (c) 72 and AoA 00. 41

Figure 29.29 Ground-mounted array: net Cp contours for lateral gap (a) 0 in, (b) 32 in and (c) 72 and AoA 315^0. 47

Figure 30 Ground-mounted array: net Cp contours for lateral gap (a) 0 in, (b) 32 in and (c) 72 and AoA 1800.. 47

Figure 31.Ground-mounted arrays: net Cp contours for lateral gap (a) 0 in, (b) 32 in and (c) 72 and AoA 215^0. 50

Figure 32.32a, 32b, 32c and 32d show the net Cp contours for wind AOAs 0^0 to AOA 3150, 225^0 and 180^0 and zero perimeter gap. 53

Figure 33.Roof-mounted arrays: net Cp contours for roof perimeter (a) 0 in, (b) 36 in and (c) 72 and AoA 0^0. 56

Figure 34.Roof-mounted arrays: net Cp contours for roof perimeter (a) 0 in, (b) 36 in and (c) 72 and AoA 315^0. 58

Figure 35.Roof-mounted arrays: net Cp contours for roof perimeter (a) 0 in, (b) 36 in and (c) 72 and AoA 180^0. 59

Figure 36. Roof-mounted arrays: net Cp contours for roof perimeter (a) 0 in, (b) 36 in and (c) 72 and AoA 2150..... 59

1. INTRODUCTION

In the last few years, the price of electricity generation has increased dramatically, especially in the state of Florida. Electricity in Florida has been for many years around 16 percent higher than the national average. Over half of the state's electricity is generated from natural gas, and 25 percent of it comes from coal. In general, Florida generates more electricity from petroleum than any other state. Florida also produces electricity from municipal solid waste and landfill gas, though the contribution from these sources to the overall state's electricity production is insignificant. In 2009, a 25-megawat solar photovoltaic plant was constructed in the state, which influenced the planning of several other solar plants statewide (Florida Energy facts). Yet, the state of Florida's energy production from solar thermal, or photovoltaic, accounts for only a 0.005% of the state's total energy generation.

The current impetus for alternative energy sources is increasing the demand for solar energy technologies in Florida and around the United States. The existing types of technologies, methods of installation, and mounting locations (ground, roof, or integrated with the building envelope) vary significantly, and are consequently affected by wind loads in different ways.

Most cities in Florida tend base construction on Chapter 16 of the Florida Building Code (FBC- 2007) for structural mounting, attachments and design of photovoltaic equipment. However, Chapter 16 of the FBC does not explicitly provide a dedicated section regarding photovoltaic installation. This lack of information related with design wind loads on photovoltaic technology results in

two kinds of oversight: (1) more of the systems are consequently over-designed, resulting in a direct increase of installation costs, and (2) the photovoltaic systems are under designed, resulting in the total destruction of equipment after an extreme wind event. The lack of prescriptive requirements as part of the FBC diminishes the opportunity for the solar panel industry to further develop. Uncertainty about what constitutes a safe and secure installation for a given wind load can complicate the approval process for a solar panel installation, thus hindering the progress of solar panel technology.

2. RESEARCH HYPOTHESIS

The effects of wind loads on solar panels could be accurately measured by using Wind Tunnel Testing techniques. It is consequently hypothesized by both developing wind tunnel tests and analyzing the data that more accurate and reliable information about wind loads on solar panels can be obtained, thus, reducing the uncertainty.

3. RESEARCH OBJECTIVES

The research objectives are to:

(i) Evaluate wind loads on a single ground mounted solar panel and

(ii) Evaluate wind loads on a ground and roof mounted arrayed solar panel using industry accepted boundary layer wind tunnel experimentation.

(iii) Assess effects of solar panel slopes on pressure coefficients.

(iv) Assess effects of solar panel terrain exposure on pressure coefficients.

(v) Assess effects of solar panel support highs on pressure coefficients.

(vi) Assess effects of spacing between arrays on pressure coefficients in solar panel arrays.

4. LITERATURE REVIEW

Considering the high demand for solar power and the variations among solar technologies available, only a limited number of wind tunnel and numerical studies exist regarding solar panel aerodynamics. Chevalien et al. (1979) performed a wind tunnel study investigating the sheltering effect on a row of solar panels mounted on a building model. Kopp et al. (2002) conducted experimental studies on the evaluation of wind-induced torque on solar arrays arranged in a parallel scheme, and demonstrated that for a separation close to the critical value where the onset of wake buffeting was anticipated, the peak aerodynamically-induced system torque was observed at a 270^0 wind angle of attack due to the formation of vortex shedding from the upstream modules. Chung et al. (2008) carried out an experimental study to investigate the wind uplift and mean pressure coefficients on a solar collector model installed on the roof of buildings under typhoon-type winds. The study found that the uplift force could be effectively reduced by using a guide plate normal to the incident wind direction, and also, by adopting a lifted model. In addition, this study demonstrated that pronounced local effects developed around the front edge, and decreased near a distance of one-third from the leading edge.

Neffba et al. (2008) at the Colorado State University, made numerical calculations of wind loads on solar photovoltaic collectors to estimate drag, lift and overturning moments on different collector support systems. These results

were compared with direct-force measurement tests obtained during wind tunnel experiments. The numerical procedure employed k-epsilon, RNG and k-omega turbulence closures to predict loads. The RNG and k-omega model approaches produced reasonable agreement with measured loads, whereas the k-epsilon model failed to replicate measurements. Numerically generated particle path lines about the model collectors strongly resembled wind tunnel smoke visualization observations.

Steenbergen et al. (2010) did a full-scale measurement of wind loads on standoff photovoltaic systems to obtain design data for standoff solar panels modules. The results indicate that for these systems, the top and bottom pressures are very well correlated. Results are now available, which can be used as a first step towards generating guidelines for the installation of standoff solar energy panels.

Banks et al. (2008) consulted on wind loads for several solar energy projects. According to these studies, the author published some articles providing guidelines to calculate wind loads on roof-mounted solar panels in the US utilizing ASCE 7-05.Uematsu et al, (2008), made several wind tunnel testings on freestanding canopy roofs in order to determine the characteristics of wind loads on this type of structures.

Tan et al. (2009) demonstrated that the wind conditions affect the performance of a solid particle solar receiver (SPSR) by convection heat transfer through the existing open aperture. The wind effect on the performance of an SPSR was investigated numerically with and without the protection of an aero

window. The independence of the calculating domain in a wind field was studied in order to select a proper domain for the numerical simulation. The cavity thermal efficiencies and the existing temperature of the solid particles was calculated and analyzed for different wind conditions. The numerical investigation of the SPSRs' performance provided a guide in optimizing the prototype design, finding out the suitable working condition and proposing efficiency enhancing techniques for SPSRs.

Hangan et al. (2009) made CFD simulations to estimate the wind loads for various wind directions on stand-alone and arrayed solar panels. Simulations were carried out for Reynolds number (Re) equal to 2, 10, 6 at different azimuthally and inclination angles. They explicitly proved that for the stand-alone cases, the bottom panels in an array were critical in terms of wind loading.

Theoharia et al. (2009) investigated the characteristics of steady-state wind loads affecting rectangular, flat solar collectors of two different sizes mounted in clusters on the flat roofs of a five-story building by testing in the boundary layer wind tunnel. A key conclusion of the study was, in comparison with isolated flat plates, that wind loads on solar collectors are significantly reduced by the sheltering effects of the first row of collectors and of the building itself. Another investigation was performed by Theoharia (2009) to determine the maximum sheltering effect of one set of panels on another set. It was observed that at a specific distance between two sets of panels, the drag coefficient for the downstream sets of panels reached a minimum.

Kurnik et al. (2010) tested the solar panel's module temperature and performance under different mounting and operational conditions, which explicitly proved that the solar panel performance depends strongly on the way modules are mounted (open-rack, ventilated or unventilated roof mounting, etc.), and the wind speeds they are exposed to.

Geurts et al. (2010) studied the effect of wind loads on roof-mounted photovoltaic array panels. The results were presented in the format of the new Euro Code on wind loads. They concluded that the current wind loading standards were not sufficient to include the most common types of active roofs.

Barkaszi et al. (2010) summarized wind load calculations for solar panel arrays using the ASCE Standard 7-05. The study provided examples that demonstrated a step-by-step procedure for approximately calculating wind loads on solar panel arrays. They also recommended that wind tunnel testing should be conducted for the most common rooftop solar panel installation to verify methods of installation and calculations.

Recently, Bitsuamlak et al. (2010) investigated four different test cases to determine the wind effects on stand-alone, ground-mounted solar panels, with a series of different wind angles of attack, and various numbers of panels. The CFD results have been compared and validated with a full-scale experimental measurement performed at the *Wall of Wind (WoW)* testing facility at Florida International University (FIU). The numerical results obtained from CFD simulations showed similar patterns of pressure coefficient distribution when compared to full-scale measurements, but the magnitude of the pressure

coefficients was generally underestimated by the numerical calculations when compared to the experimental results. The solar panels experienced the highest overall wind loads for 180^0 wind angle of attack. The study also demonstrated that a prominent sheltering effect caused by upwind solar panels substantially reduced the wind loads on the adjacent solar panel when they are arranged in tandem.

5. METHODOLOGY

5.1. Boundary layer wind tunnel setup and flow characteristics.

For the present study, the aerodynamic characteristics of solar panel modules under atmospheric boundary layer flow conditions were investigated. The lower part of atmospheric boundary layer was simulated in the boundary layer wind tunnel at a length, velocity and time scales of 1:20, 1:4, and 1:5, respectively. The boundary layer wind tunnel facility was used to simulate a mean speed and various turbulence profiles of the natural wind approaching a building model. The facility has a long working section with a roughened floor, and turbulence-generating spires were installed at the upwind end. In the present study, floor roughness and spires have been selected to simulate open and suburban wind profiles. Open wind profiles were generated by a combined effect of 15in x 19in (38.1cm x 48.3cm) spire and 1.5in (3.81cm) triangular-floor roughness elements, while suburban wind profiles were generated by a combination of 18in x 18in (45.72cm x 45.72cm) spires with 4in (10.16cm) floor roughness elements. Figure 1 shows the wind velocity and turbulence intensity profiles as well as the spectra examples for open terrain exposure.

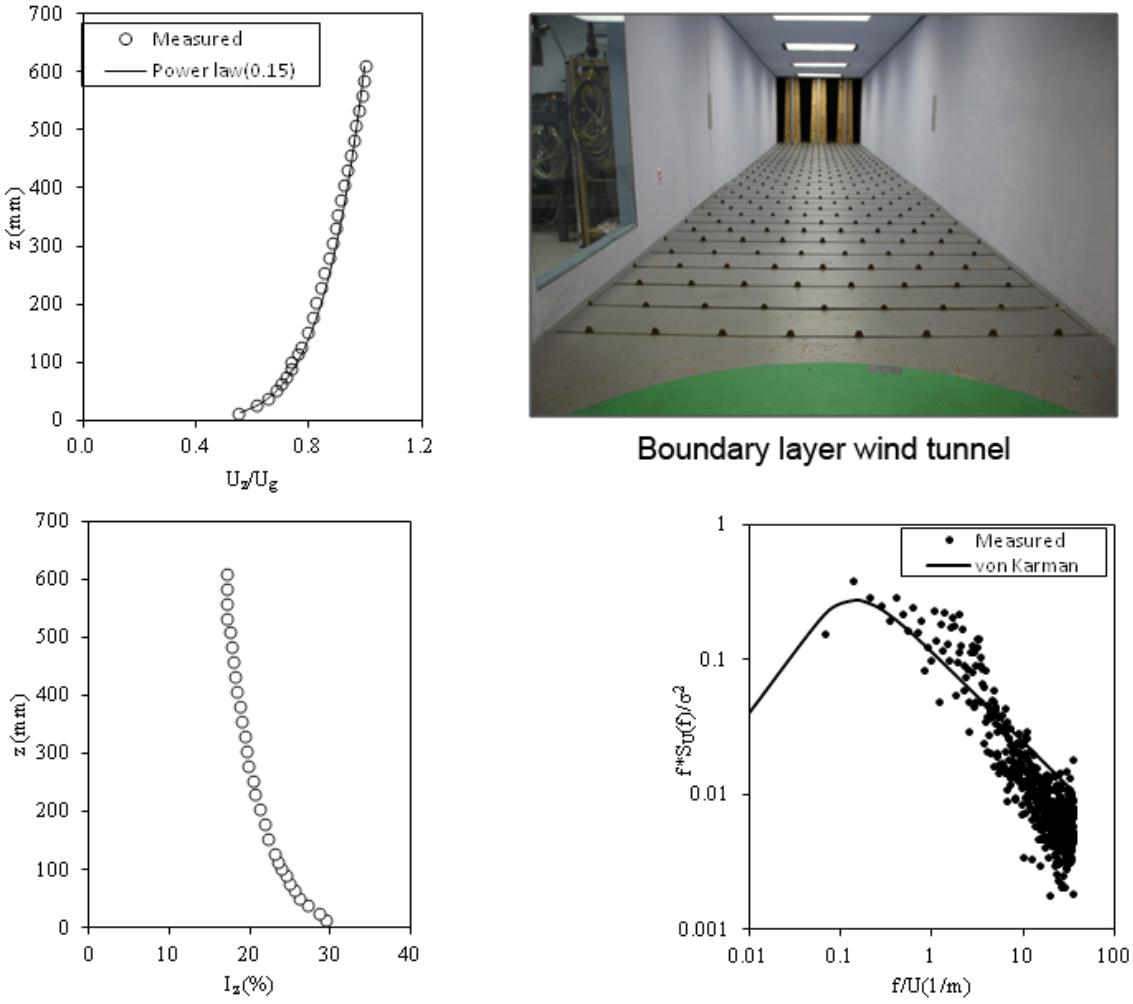

Figure 1

Trapezoidal planks and triangular floor roughness elements used to develop open exposure for the bottom 30 m, mean wind speed profile, turbulence intensity profile, and longitudinal turbulence spectrum at 1.5in (3.81cm) height in the mode.

5.2. Isolated solar panel: study wind tunnel model and instrumentation.

The isolated solar panel model was constructed in a scale of 1:20 to represent a 30ft x 4.4ft (9.14m x 1.34m) at full-scale and tested at RWDI's 7ft x 8.1ft (2.13m x 2.46m) boundary layer wind tunnel facility in Miramar, Florida. The model was tested in the absence of surroundings. The models were cut out from Plexiglas acrylic sheets using a high precision laser cutting machine, and the pressure tubes were glued with fast setting solvent cement. They were placed at 43.5ft (13.3m) down-stream of the tunnel entrance at the center of a 7.5ft (2.3m) diameter turn-table. Figure 2 shows the wind tunnel model for isolated solar panel.

Figure 2

Isolated solar panel model in a boundary layer wind tunnel in a testing position.

Solar panels with five different slopes (i.e. 0^o, 10^o, 20^o, 25^o, 30^o, and 40^o) expected to cover optimal orientations for different locations (latitudes) and three different leg heights, i.e. 12 in (30.48 cm), 24 in (60.96 cm) and 32 in (81.28 cm); short legs were considered in the study. Figure 3 summarizes the tested slope and support height cases. Each combination of slope and leg height was tested for wind angle of attacks (AoA) ranging from 0^o to 350^o at 10^o intervals. In addition, 45^o and 135^o AoA have been tested for all cases. The following nomenclature where slopes and short leg heights will be designated by the prefixes 'S' and 'H' followed by their corresponding values has been adopted. For instance, S25H12 is 25^0 slope and 12 inches short leg height. Each combination of slope and leg height was tested also for both open and suburban profile.

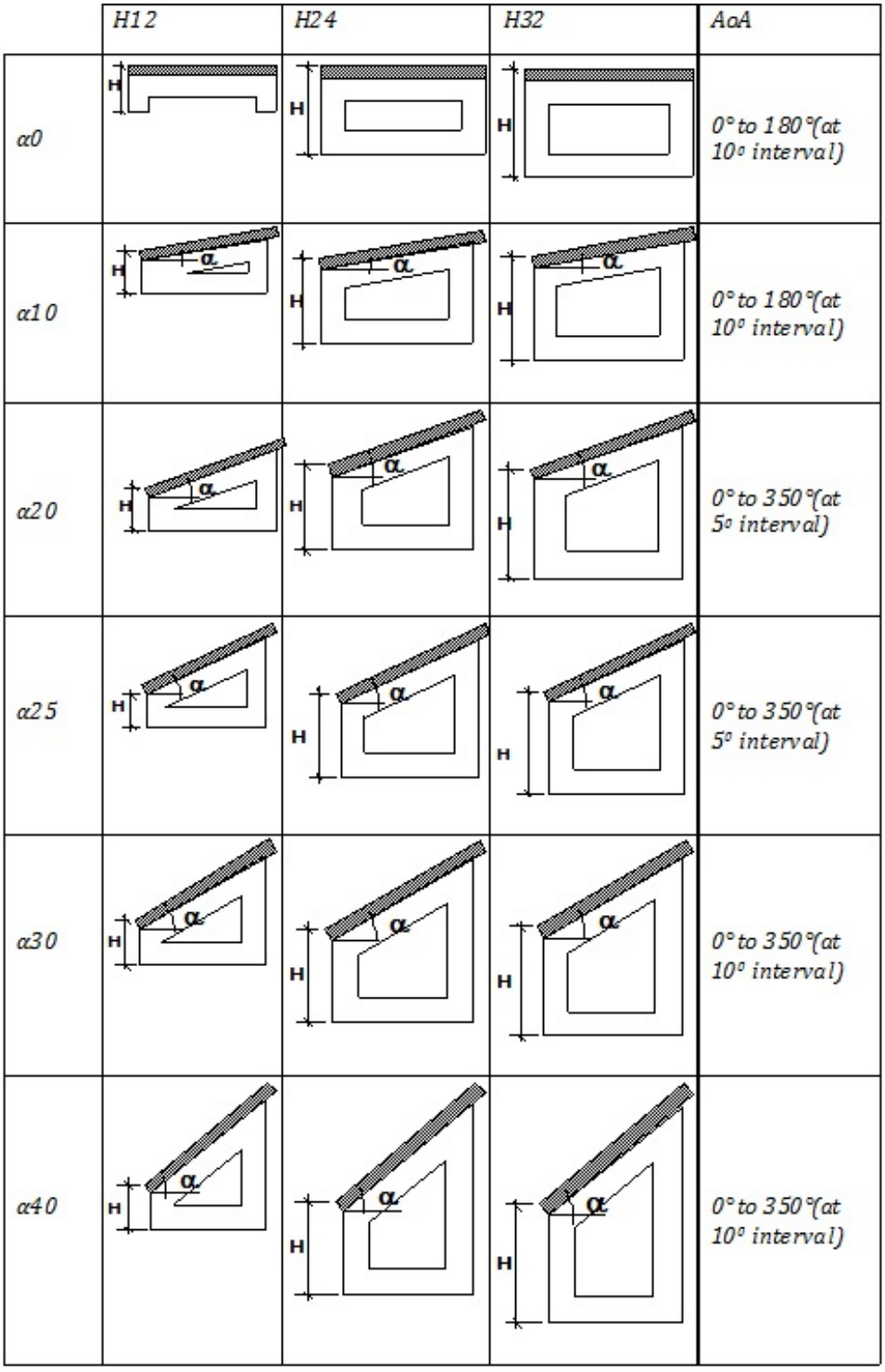

Figure 3

Isolated solar panel slopes and support heights considered in the study.

Pressure distribution on the panel surface was obtained from 80 taps installed at 40 points on the panel surface for the Single Ground mounted solar panel, (two at each point, one on the top and the other on the bottom surface) as shown in Fig. 4.

Figure 4

Pressure taps distribution used for Single PV model.

Pressure readings were taken by connecting the pressure taps to *Scani-Valve* (intelligent pressure and temperature measuring module) with 0.053in (1.34mm) solar panels C tubes for a duration of a 90-second period, at a sampling frequency of 512Hz. Consequently, a total of 46,080 measurement points were collected for each angle, providing enough information for each particular case tested. The data collected is low-pass filtered to reduce resonant effects resulting from the tubes using a transfer function developed specifically for the tubes used.

The Scani-Valve equipment consisted of eight coupling input connections, each with a 64-channel capacity. Since it had 80 taps installed, for the Single Ground Mounted solar panel, 80 channels of the Scani-Valve where connected to the model. Each channel generated a column of data, and the pressure was measured in psi 46,080 times for each angle following the frequency that has been explained above.

A similar procedure was use for both Ground Mounted Arrayed solar panels and Roof Mounted solar panels. As it was mentioned above, the model used for testing Ground Mounted Arrayed solar panel and Roof Mounted solar panel had 48 taps. In this case, a total of ten instrumented panels were placed in the wind tunnel. Accordingly, a total of 480 channels where connected to the Scani-Valve, and each channel generated a column of data of pressure measured in psi.

5.3. Solar Panel Array: Wind Tunnel Study Model and Instrumentation

5.3.1. Ground-Mounted Arrayed Solar Panel:

For the ground-mounted arrayed solar panel, ten solar panel models were constructed at a 1:30 scale to represent a 30ft x 4.4ft (9.14m x 1.34m) panel at full-scale and tested at RWDI's 7ft x 8.1ft (2.13m x 2.46m) in the boundary layer wind tunnel facility in Miramar, Florida. Several dummy models, i.e. without instrumentation but having similar geometry with the instrumented ones, were used to create "arrayed" surrounding conditions. The height of the shortest leg of the support was fixed in order to represent a 32 inch high full scale, and the slope of the solar panel was set to 25 degrees. The models were cut out from Plexiglas acrylic sheets using high a precision laser cutting machine, and the pressure tubes were glued with fast setting solvent cement. They were placed at 43.5ft (13.3m) down-stream of the tunnel entrance at the center of a 7.5ft (2.3m) diameter turn-table. Figure 5 shows the ground-mounted array considered in the present study.

Figure 5

Ground-mounted arrayed solar panel model in a boundary layer wind tunnel in a testing position.

Pressure distribution on the panel surface was obtained from 48 taps installed at 24 points on the panel surface for the ground mounted arrayed solar panel (two at each point, one on the top and the other on the bottom surface) as shown in Fig. 6.

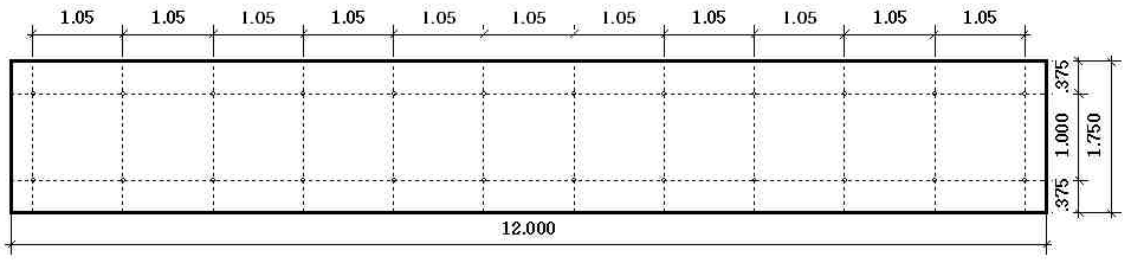

Figure 6

Pressure-taps distribution used for both, ground and roof-mounted model.

Note: For arrayed case a total of ten PV panels were instrumented simultaneously with this tap distribution for each test case.

A pressure measurement procedure similar with the one described for the isolated solar panel was used for ground-mounted arrayed solar panel. As it was mentioned above, the model used for testing the Ground Mounted Arrayed solar panel and Roof Mounted solar panel had 48 taps. In this case, a total of ten instrumented panels were placed in the wind tunnel. Accordingly, a total of 480 channels were connected to the Scani-Valve, and each channel generated a column of data of pressure measured in psi.

Longitudinal distance between the solar panel: Three different longitudinal distances between each panel to represent 24, 48 and 72 inches (61,122 and183 cm)

at full scale were investigated (refer Fig. 7). During the wind tunnel testing, the center of the footprint area of the ten panels was placed in the center of the 7.5ft (2.3m) diameter turn-table.

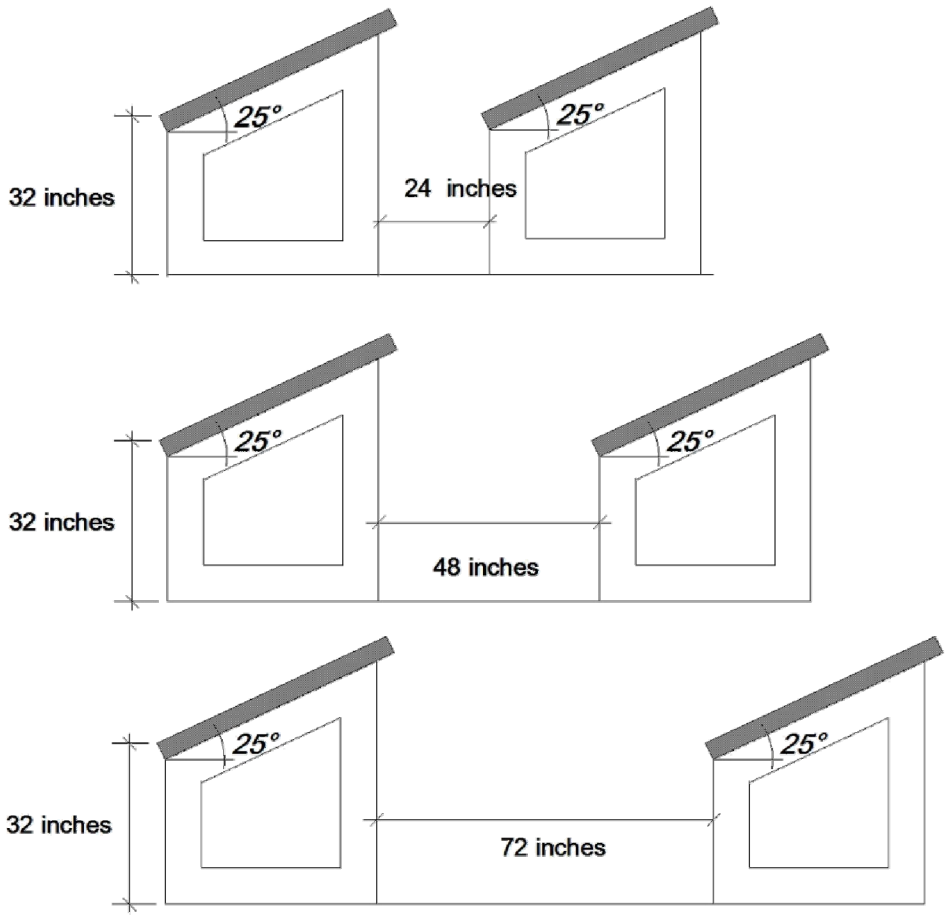

Figure 7

Ground-mounted solar panel: Longitudinal distances investigated in the wind tunnel.

Lateral gap between the solar panel: Three different lateral gaps between each ground –mounted solar panel to represent 0 inches, 36 inches(91.44 cm) and 72 inches (183 cm)at full scale were investigated (refer Fig. 8).

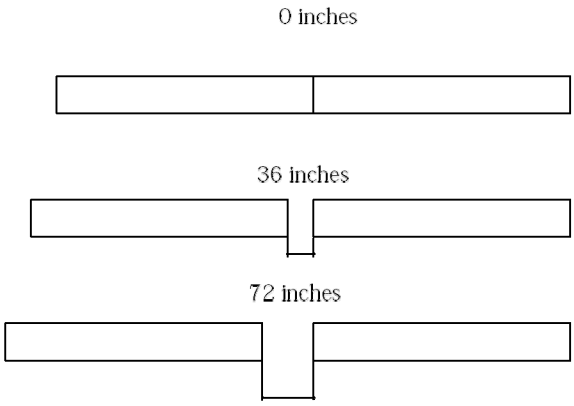

Figure 8

Ground-mounted solar panels: Lateral gaps investigated in the wind tunnel.

Test configuration: The ground-mounted array considered in the present study is shown in Fig 9. The critically loaded solar panels would be the ones located at the corners. Due to symmetry, only the north-east and south-east corners were investigated in the present study, i.e. regions I and II shown in Figure 9 respectively. Due to the enormous array size, it was not possible to instrument all the three columns in the north-east test at the same time. At the time of testing the Scani-Valve capacity was limited to 500 channels, sufficient only for connecting 10 solar panels at a time. Also it was necessary to test the array in parts as described below due to the lack of enough room in the boundary layer wind tunnel for testing all arrays together.

However by systematically testing configuration 1, 2 and 3 separately as shown in Fig 10 a, b and c respectively and putting the test result together, the

North–east corner could be covered. Similarly, by systematically testing configuration 4, 5 and 6 separately as shown in Fig 10 d, e and f respectively and putting the test result together, the South–east corner was covered. The ten-instrumented panels were tested together with other dummy panels (non-instrumented panels) for six different configurations as it is shown in Fig. 10.

Each configuration is further described in detail below. Each combination of longitudinal distances and lateral gaps were tested in six different configurations, and each one was tested for different wind angles of attack (AoA).

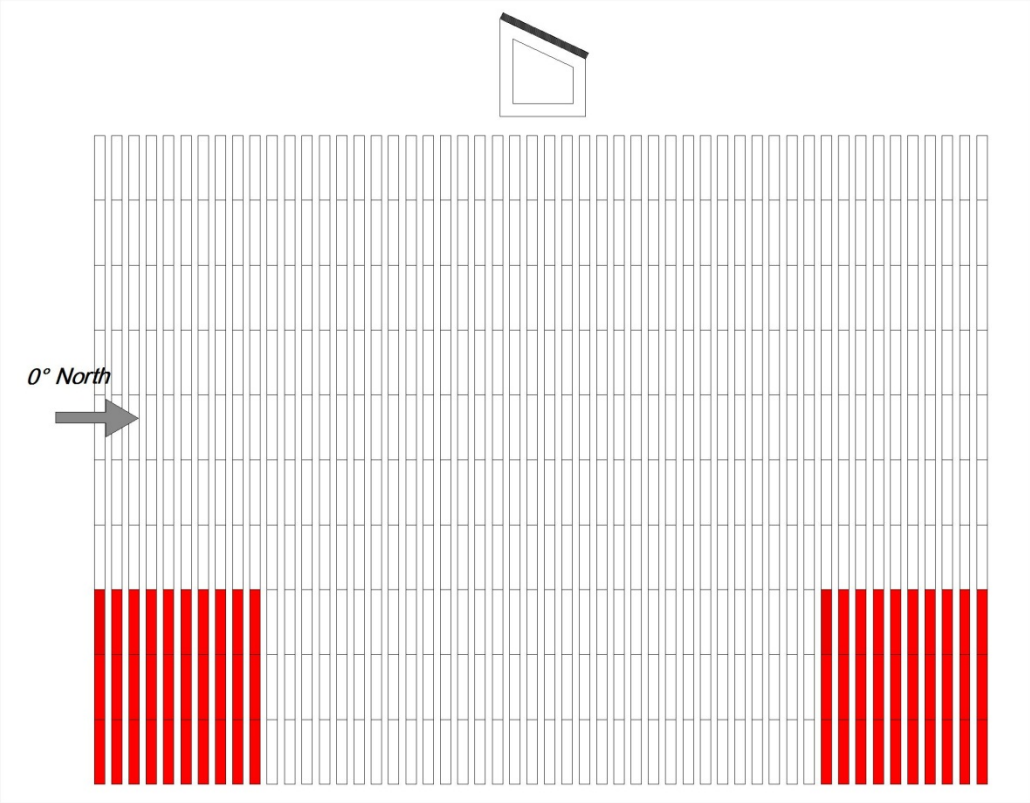

Figure 9

Ground-mounted arrays considered in the present study.

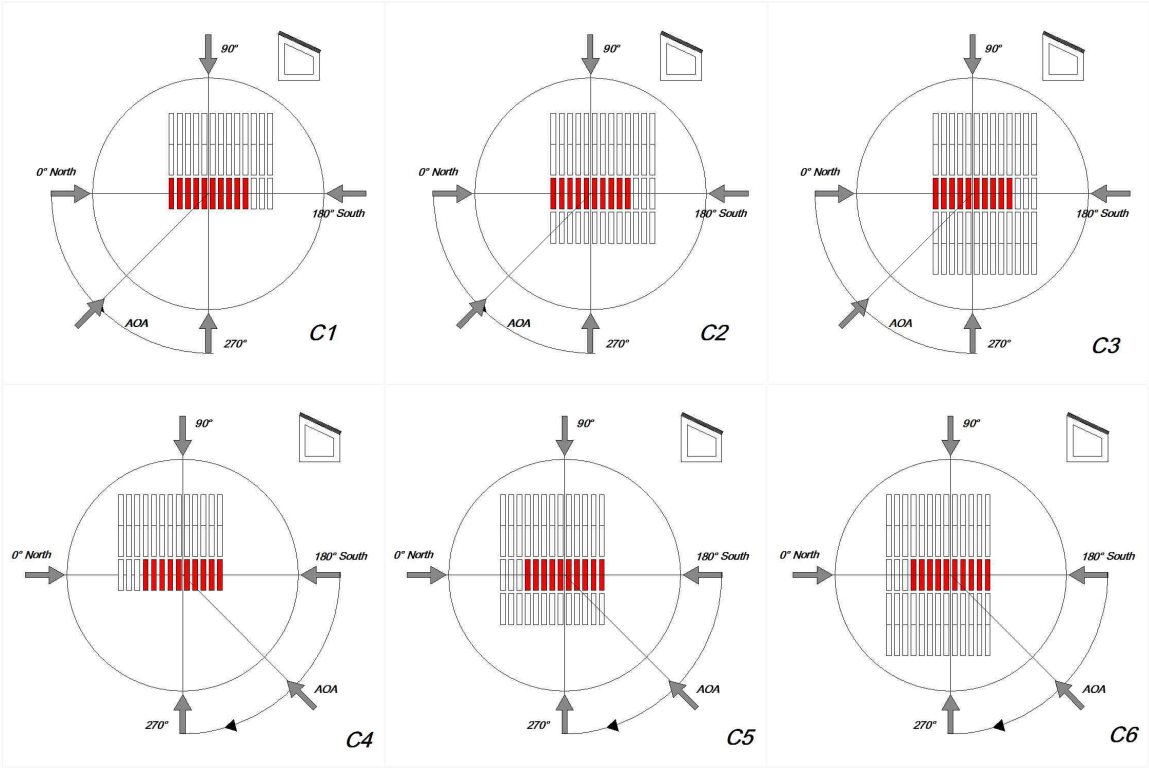

Figure 10

Ground-mounted array test configuration definition.

Configuration C3 was a result of setting the ten-instrumented panels between two equal and symmetrically distributed groups of non-instrumented panels. Each group consisted of 26 non-instrumented panels. The short leg height of the instrumented panel faces south (180^0 wind direction). This configuration was tested from 0 degrees to 90 degrees.

Configuration C2 was a result of setting the ten-instrumented panels (marked in red in the figure) between two groups that were not instrumented panels. The western group consisted of 26 non-instrumented panels as it is shown in figure 10.

The eastern group consisted of 13 non-instrumented panels as it is shown in figure 10 .The short leg height of the instrumented panel faced south (180 degree wind direction). This configuration was tested from 270 degrees to 0 degrees.

Configuration C1 was a result of setting the ten instrumented panels together with 26 non-instrumented panels as it is shown. The short leg height of the instrumented panel faces south (180^0 wind direction). This configuration was tested form 0 degrees to 270 degrees. It should be mentioned that for each of the three above described configurations C1, C2, and C3, a set of three non-instrumented panels were placed behind the 10 instrumented panels as it is shown.

Configuration C6 was a result of setting the ten-instrumented panels between two groups equals and symmetrically distributed not-instrumented panels. Each group consisted of 26 non-instrumented panels as it is shown. The short leg height of the instrumented panel faces south (180^0 wind direction). This configuration was tested from 180 degrees to 270 degrees.

Configuration C5 was result of setting the ten-instrumented panels between two groups of non-instrumented panels. The western group consisted of 26 non-instrumented panels as it is shown. The eastern group consisted of 13 non-instrumented panels as it is shown. The short leg height of the instrumented panel faces south (180^0 wind direction). This configuration was tested from 180 degrees to 270 degrees.

Configuration C4 was a result of setting the ten instrumented together with 26 non-instrumented panels as it is shown. The short leg height of the instrumented

panel faces south (180 degree wind direction). This configuration was tested from 180 degrees to 270 degrees.

5.4. Roof-mounted arrayed solar panel

For the Roof Mounted solar panel*;* ten solar panel models were constructed at a 1:30 scale. The panels were separated to represent 48 inches longitudinal distance at full scale between them. The height of the panel's supports was fixed to represent 32 inches (91.44 cm) at full scale short legs. The center of the footprint area of the ten panels was placed in the center of the 7.5ft (2.3m) diameter turn-table. They were mounted on a building model cutout from Plexiglas acrylic sheet to represent a width of 90ft, a length of 117ft, and 18.5ft high building (see Fig. 11). A number of 35 (non-instrumented) 30ft x 4.4ft (9.14m x 1.34m) model panels were used in order to simulate the surrounded solar panels. They were also mounted on a similar building model.

Figure 11

Roof-mounted arrayed solar panel model in a boundary layer wind tunnel in a testing position.

Pressure distribution on the panel surface was obtained from 48 taps installed at 24 points on the panel surface for the roof-mounted arrayed solar panels (see Fig. 6). A pressure measurement procedure similar with the one described for isolated solar panel and for ground-mounted arrayed solar panels was used here as well.

Test configuration: The roof-mounted array considered in the present study is shown in Fig 11. Due to symmetry, only half of the roof area needs to be tested. Again, due to the enormous array size, it was not possible to instrument all three columns at the same time. Hence test configurations 1, 2, 3 and 4 described in Fig 12 were adopted. The configurations were set by modifying the position of the non-instrumented panels in relation with the ten instrumented panels (see Figure 12).

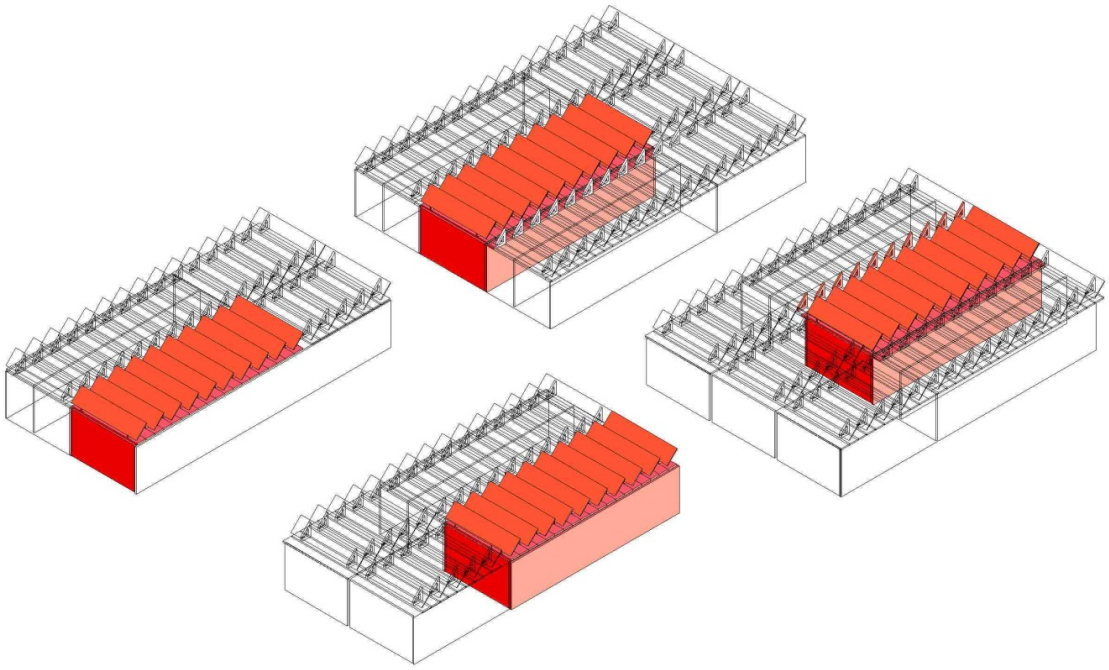

Figure 12

Roof-mounted arrays basic test configuration definition.

Another parameter considered for the roof-mounted solar panels array was the "roof perimeter gap". Three different roof perimeter gaps, referred here after simply as "perimeter gaps", representing 0, 36 and 72 inches (0,92 and 183 cm) at full scale between them were considered as shown in Fig. 13. Adding a walking area to the building perimeter modified each configuration. The walking area modified the distance between the solar panels and the building perimeter. The walking areas were made to represent both 36 inches and 72 inches (92cm and 183 cm) at full scale. The modification described previously resulted in a total of eight test-configurations as it is shown at Fig. 14, where each combination of roof perimeter-gaps were tested in four different configurations and each one was tested for different AoA.

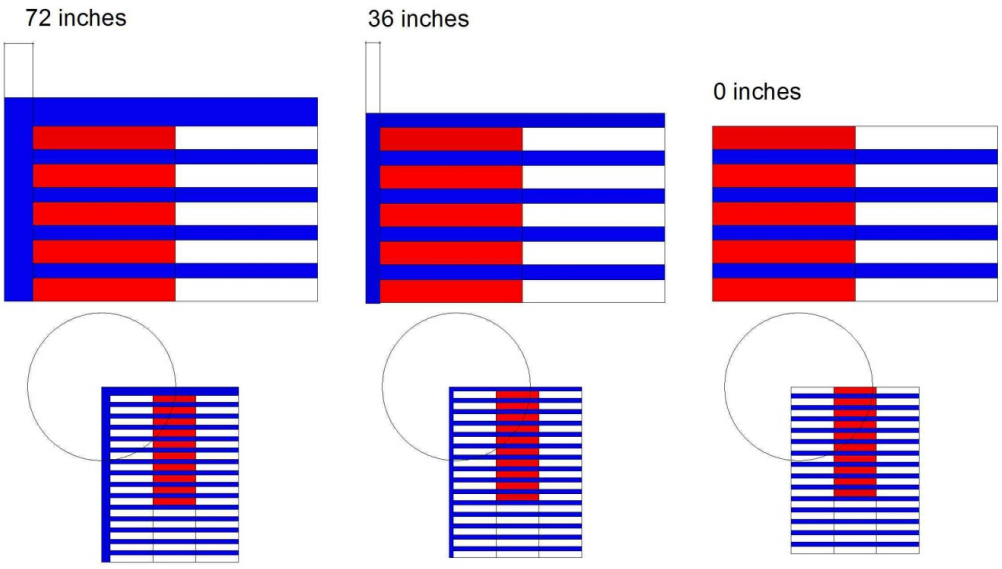

Figure 13

Perimeter gaps considered for roof-mounted solar panel array.

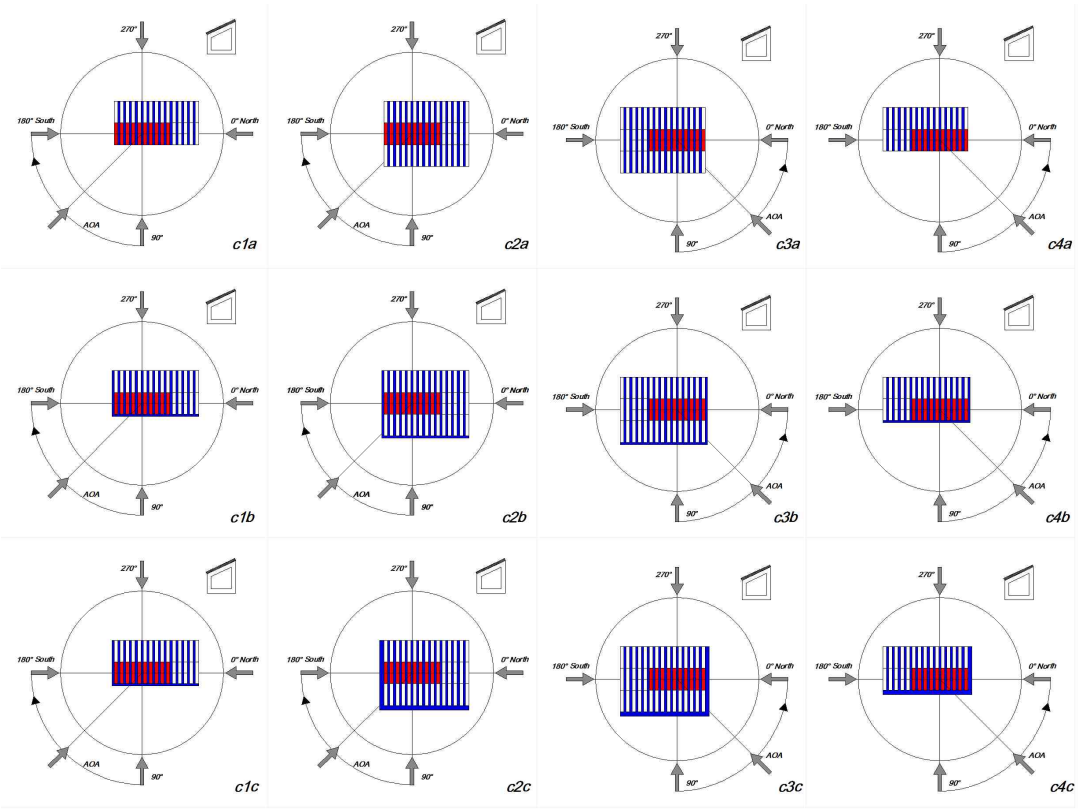

Figure 14

Total roof-mounted array test configurations.

Configurations c2a, c2b, c2c, were the result of setting the ten instrumented panels (marked in red in the figure) between two groups of equals and symmetrically distributed non-instrumented panels. Each group consisted of 15 non-instrumented panels. 5 non-instrumented panels more were added in order to keep the configuration symmetrical, in order to cover the northern windward side as it is shown. The short leg height of the instrumented panel faces south (180^0 wind direction). This configuration was tested from 90 degrees to one 180 degrees, and also the one 135 degree angle was tested.

Configurations c1a,c1b,c1c were the result of setting the ten instrumented panels (marked in red in the figure) beside one group of 15 non-instrumented panels

covering the western windward; 5 more not instrumented panels were added in order to keep the configuration symmetrical, and in order to cover the northern windward side as it is shown. The short leg height of the instrumented panel faces south (180 degree wind direction). This configuration was tested from 90 degrees to 180 degrees, and also the 135 degree angle was tested.

Configurations c3a, c3b, c3c were the result of setting the ten instrumented panels (marked in red in the figure) between two groups of equal and symmetrically distributed non-instrumented panels; each group consisted of 15 non-instrumented panels; 5 more non-instrumented panels were added in order to keep the configuration symmetrical and in order to cover the southern windward side as it is shown. The short leg height of the instrumented panel faces south (180^0 wind direction). This configuration was tested form 0 degrees 90 degrees, and also the 45 degree angle was tested.

Configurations c4a,c4b,c4c were the result of setting the ten instrumented panels (marked in red in the figure) beside one group of 15 non-instrumented panels covering the western windward; 5 more non-instrumented panels were added in order to keep the configuration symmetrical, and in order to cover the southern windward side as it is shown. The short leg height of the instrumented panel faces south (180^0 wind direction). This configuration was tested from 90 degrees to 180 degrees, and also the 135 degree angle was tested. As it has been mentioned previously, each of the four configurations above was briefly modified by adding a walking area to the building perimeter. The walking area modified the distance between the solar panel and the building perimeter.

6. RESULTS AND DISCUSSIONS

6.1. Wind pressure coefficient.

As it has been mentioned above the pressure readings were taken by connecting the pressure taps to the Scani-Valve, and each tap generated a column of data. The pressure was measured in psi 46,080 times for each angle following the frequency that has been explained above. The data was analyzed in order to evaluate the wind pressure coefficients. The pressure coefficients were referenced to the middle height *h* of the model panel (see Fig. 15). Once the velocity was gotten the *q* reference was calculated by using the equation *q* reference = $\frac{1}{2}\rho V^2$. The *q* reference value was used in order to calculate the pressure coefficients (C_p) value for each pressure measured; it was done by simply dividing the pressure measured by the q reference value.

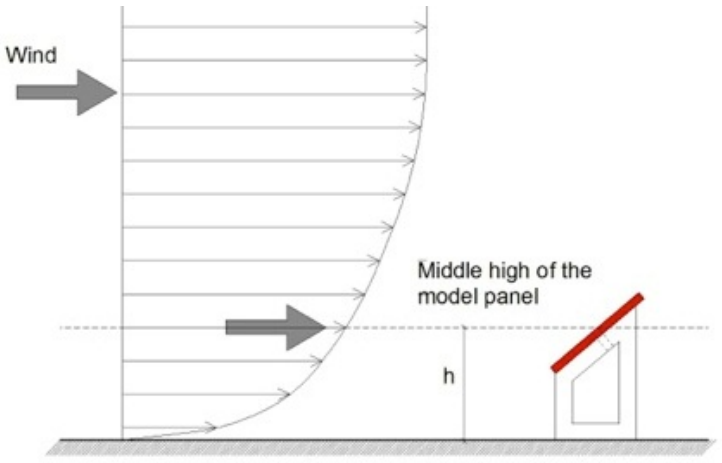

Figure 15

Wind profile, and reference height definition.

Once the C_p values were calculated for each tap a net C_p value was calculated by adding both the C_p value for the tap on the top, and the C_p value for the tap on the bottom surface. A statistical analysis was performed after. The statistical analysis resulted in valuable information that explicitly shows the maximum C_p, the minimum C_p, and the mean C_p for each pressure measurement point (taps) on the solar panel.

6.2. Single Ground Mounted Solar Panel

As it has been previously mentioned, the data obtained for the Single Ground Mounted solar panel included the four variables: Wind Profile (Open or Sub), height of the support, slope of the panel, the wind direction (AoA); also three main statistical analyses were done with the C_P value obtained from the pressure analysis: Maximum (Net), Minimum (Net), and Average Net C_P value. The net value was obtained by adding the top and bottom tap measurement (vector addition) at each measuring points as defined in Fig. 4.

Parametric analysis of the wind load on the single ground mounted solar panel was made by fixing one of the variables, and performing a comparative analysis on the others. Comparative analysis of the wind load on the single ground mounted solar panel includes: different AoA; the same AoA (worst cases) but for different heights of the support (H); the same AoA (worst cases) but for different slopes (S); and the same AoA (worst cases) but for different Wind Profiles (Open, Suburban).

6.2.1. Variation of wind pressure coefficients with wind angle of attack (AoA)

A solar panel with a slope of 25 degrees, and H = 32in was selected to show the variation of the pressure coefficients for different wind AoA. This slope was selected as it is more representative for South Florida's latitude. Figures 15 and 16

show the net C_p three dimensional plots for the solar panels with 25^0 slope and for wind AoAs of 0^0 to AoA of 360^0 at 45^0 steps. These figures (i.e. Figs 16a to h) are explicitly showing the effect of the variation of the AoA on the solar panels' C_P value. The worst wind AoAs appears to be 45^0, and 180^0. Wind AoA of 135^0 which is symmetrical with 45^0 is also critical.

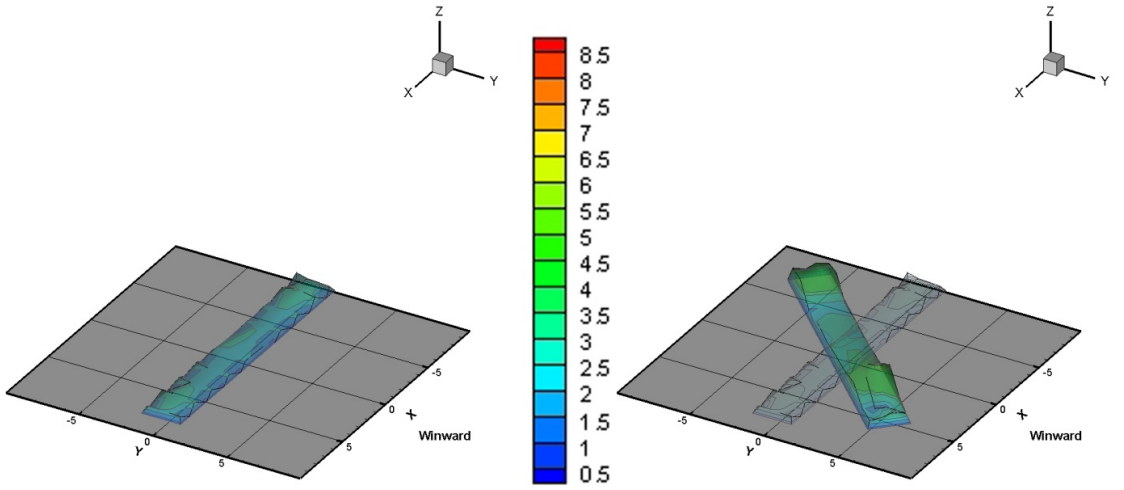

AoA 0^0 and AoA 45^0

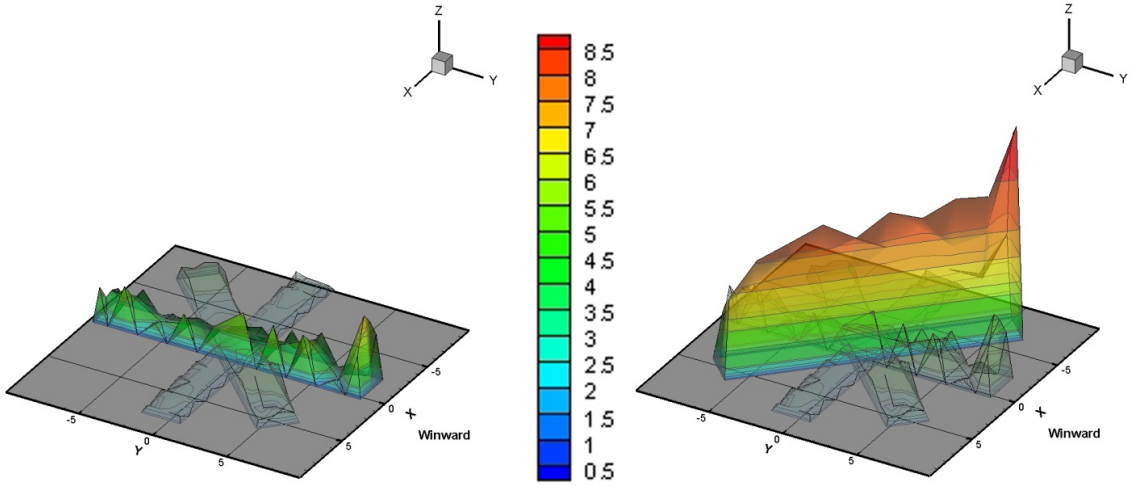

AoA 90^0 and AoA 135^0

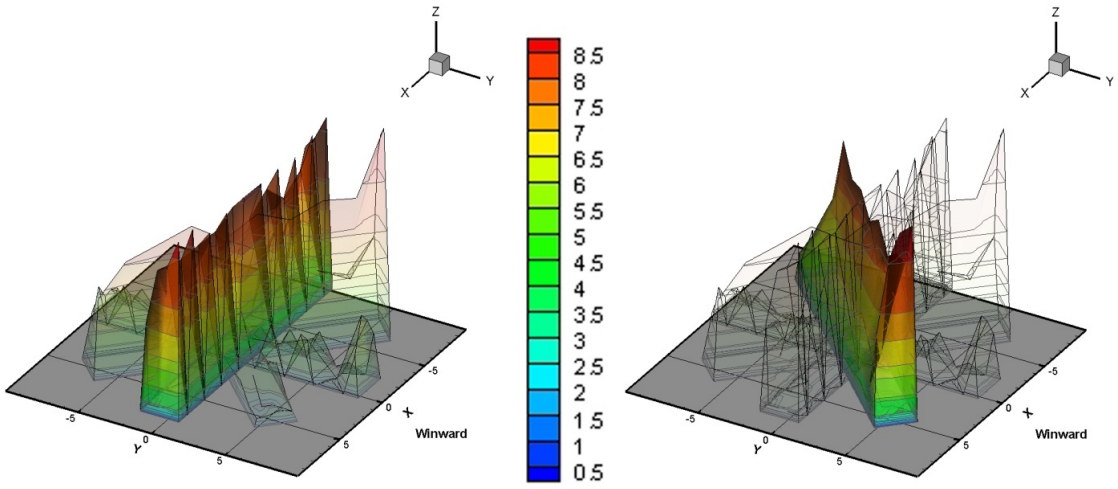

AoA 180^0 and AoA 225^0

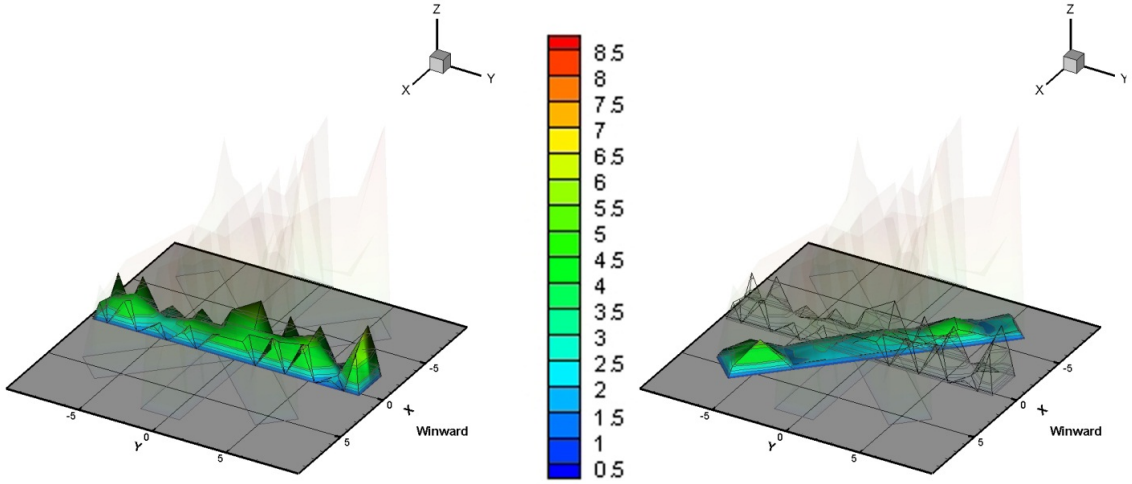

Figure 16

Maximum Cp Plots for (a) 0^o (b) 45 ^{o} (c) 90 ^{o} (d) 135^0 (e) 180^0 (f) 225^0 (g) 270 ^{o}, and (h) 315^o wind AoAs.

AoA 270^0 and AoA 315^0

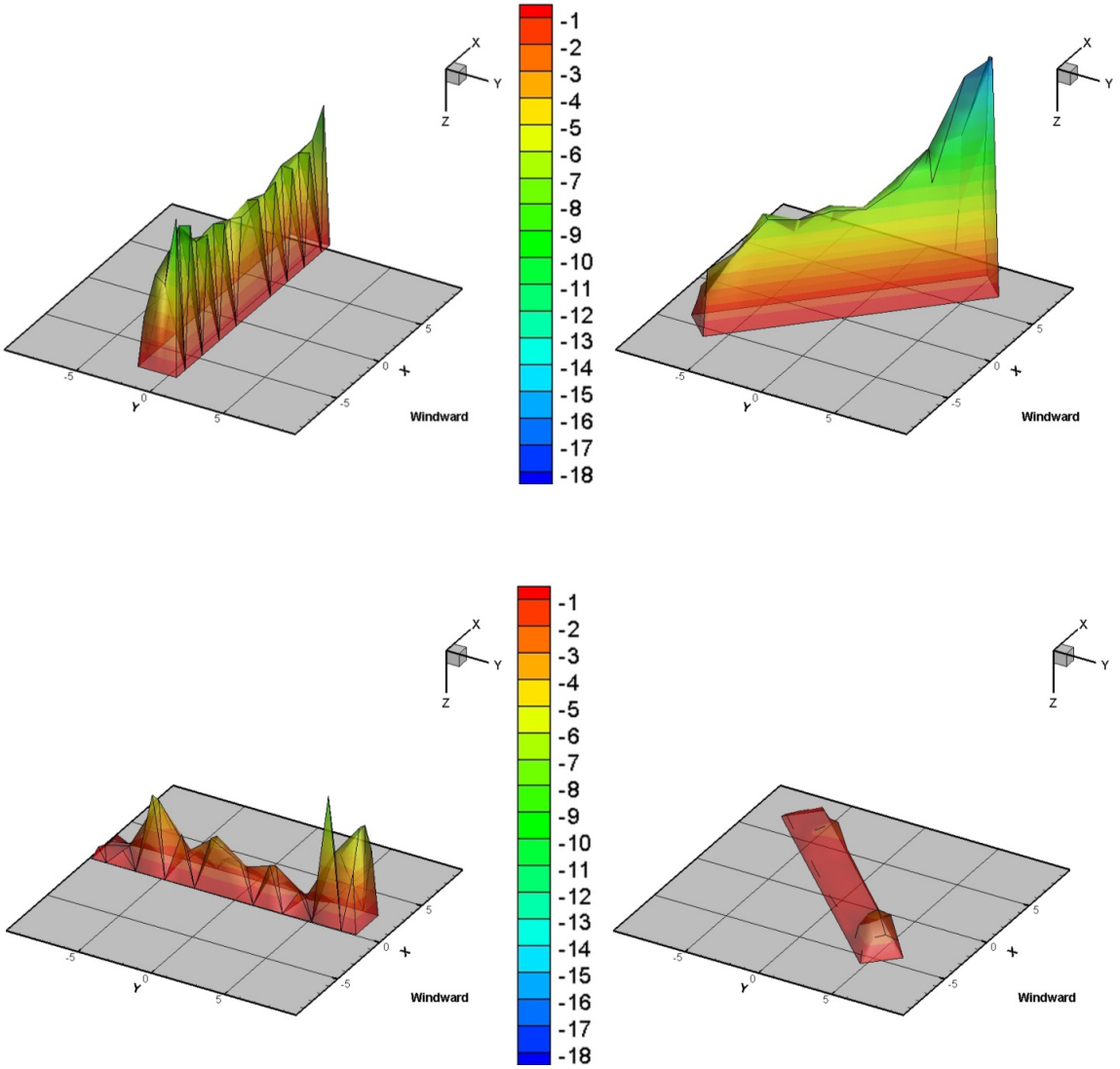

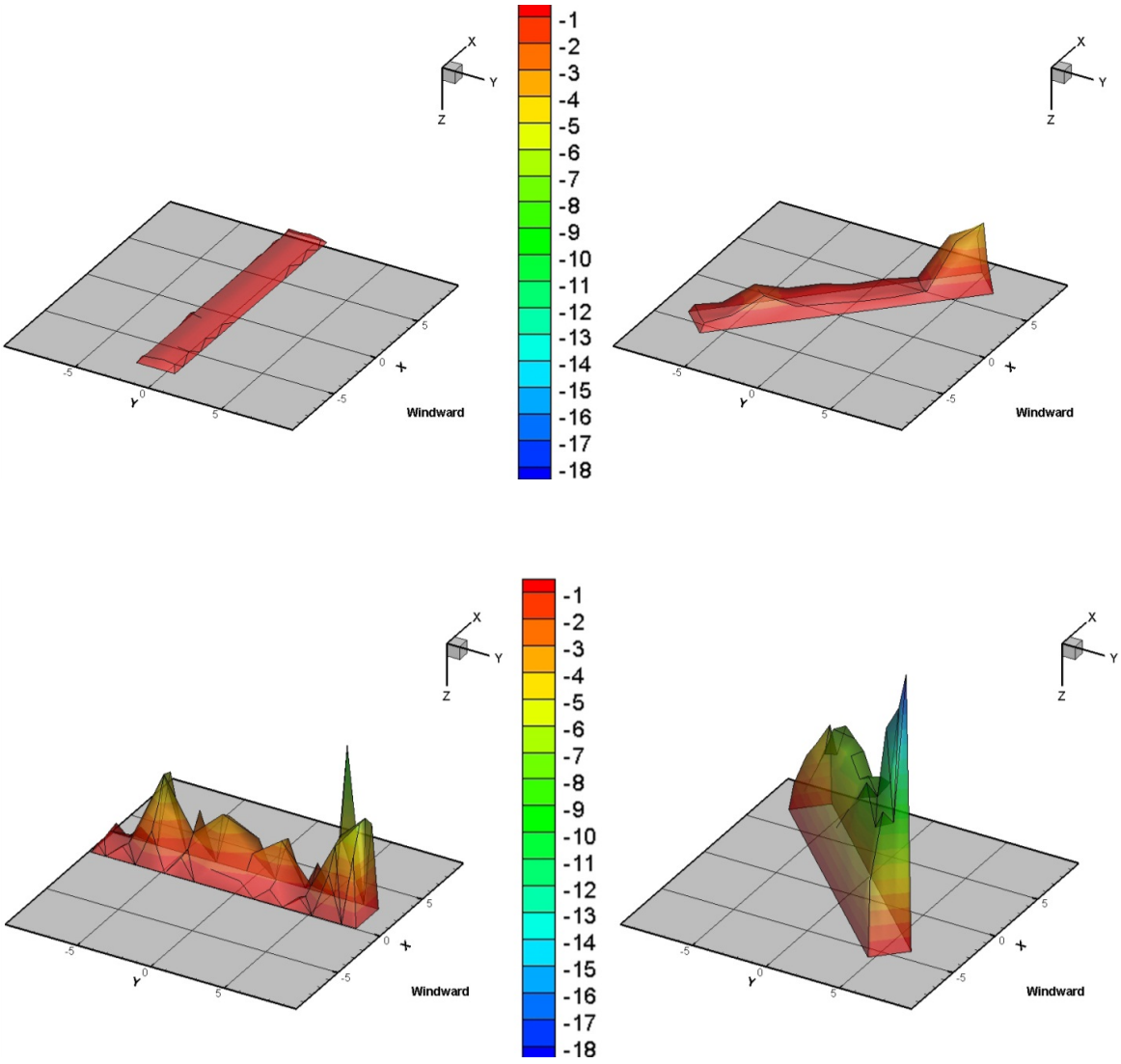

Figure 17

Minimum Cp Plots for (a) 0^{o} (b) 45 ^{o} (c) 90 ^{o} (d) 135^{0} (e) 180^{0} (f) 225^{0} (g) 270 ^{o}, and (h) 315^{o} wind AoAs.

6.2.2. Effects of support heights (H) on wind pressure coefficients

To study the effects of support height the worst wind AoAs, 180^{0} and 45^{0} for the three different support heights (H=12, 24, and 32 in) were considered. Figures 18a and 18b show both the mean and the maximum C_P value for an AoA of 180^{0}, the slope of the panel was 25 degrees and the wind profile was open. Figures 19a and

19b show both the mean and the maximum C_P value for an AOA of 45^0, the slope of the panel was 25 degrees and the wind profile was open. The three dimensional contour comparison both for 45^0 and 180^0 wind AoAs clearly shows no major variations for the different heights of the support. Thus it can be concluded that the support height does not have significant effect on wind loads for support height variations similar to the present case.

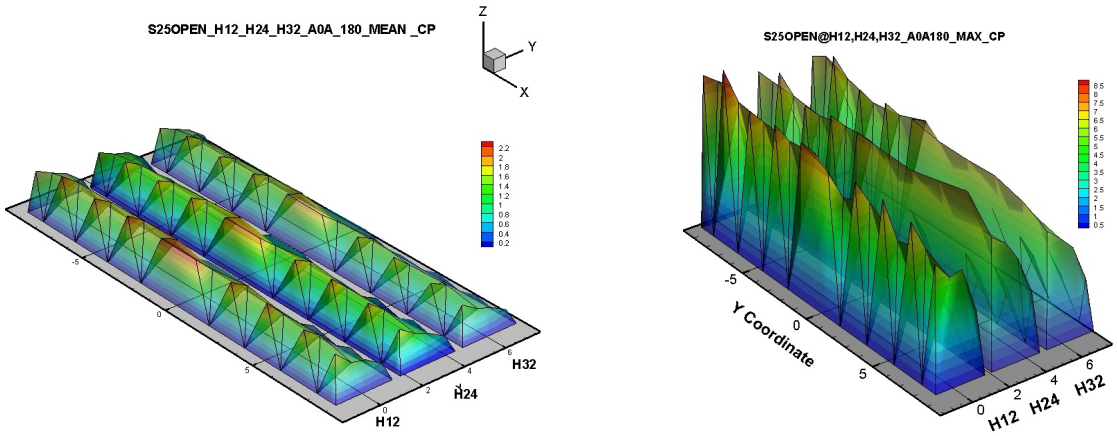

(a) (b)

Figure 18

(a) Mean Cp for H12, H24, and H32 and wind AoA 1800 and (b) maximum Cp for H12, H24, and H32 and wind AoA 1800.

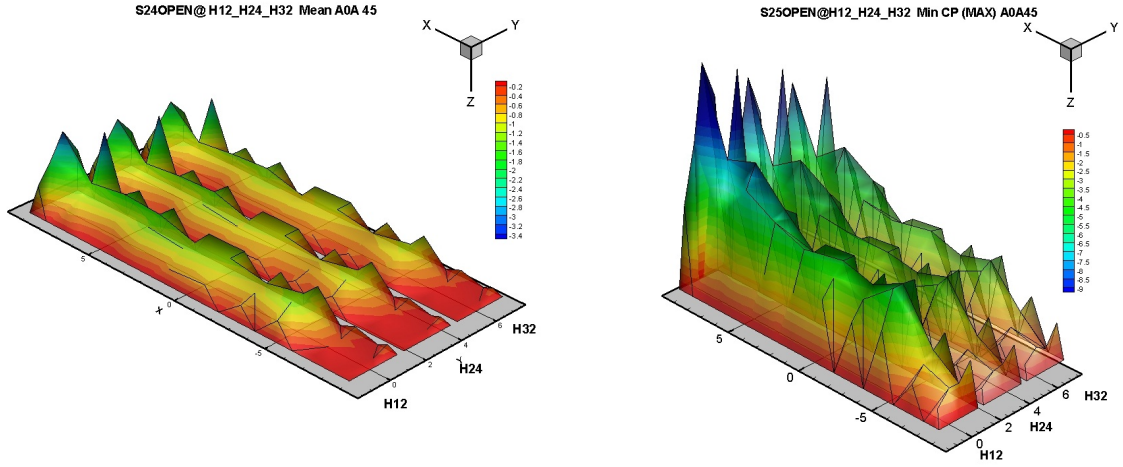

(a) (b)

Figure 19

(a) Mean Cp for H12, H24, and H32 and wind AoA 45^0 and (b) Maximum Cp for H12, H24, and H32 and wind AoA 45^0.

6.2.3. Effects of Solar Panel Slope (S10, 20, 25, 30 And 40) On Wind Pressure Coefficients

To study the effects of solar panel slope, the worst wind AoAs, 45^0 and 180^0 for a case with support height H=32in were considered. Figures 20 and 21 show both the mean and the maximum CP value for an AOA of 45^0 and 180^0, respectively. The slope of the solar panels was 25 degrees and the wind profile was open.

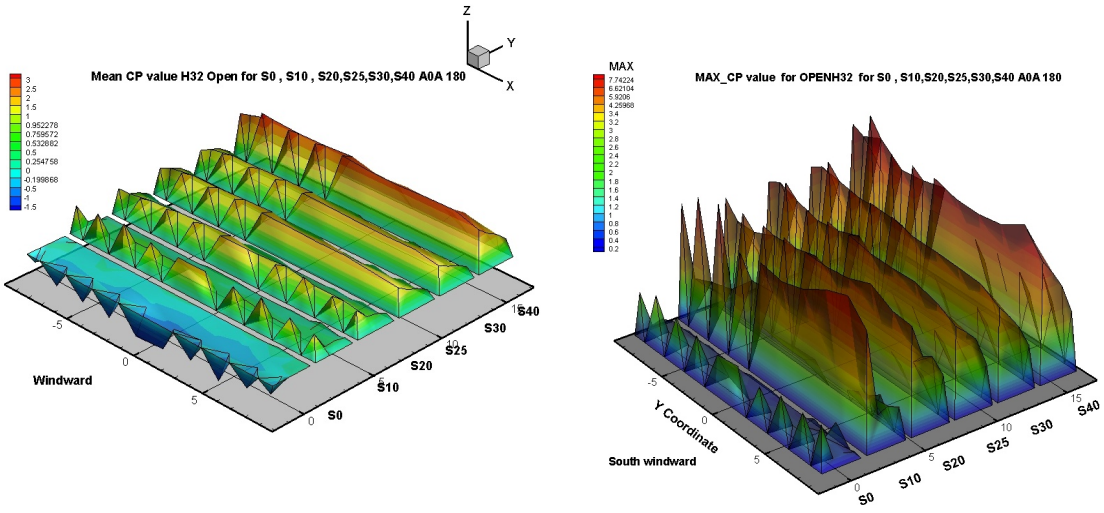

(a) (b)

Figure 20

(a) Mean Cp for S10, S20, S25, S30 and S40 and wind AoA 180^0 (open terrain), and (b)Maximum Cp for S10, S20, S25, S30 and S40 and wind AoA 180^0 (open terrain).

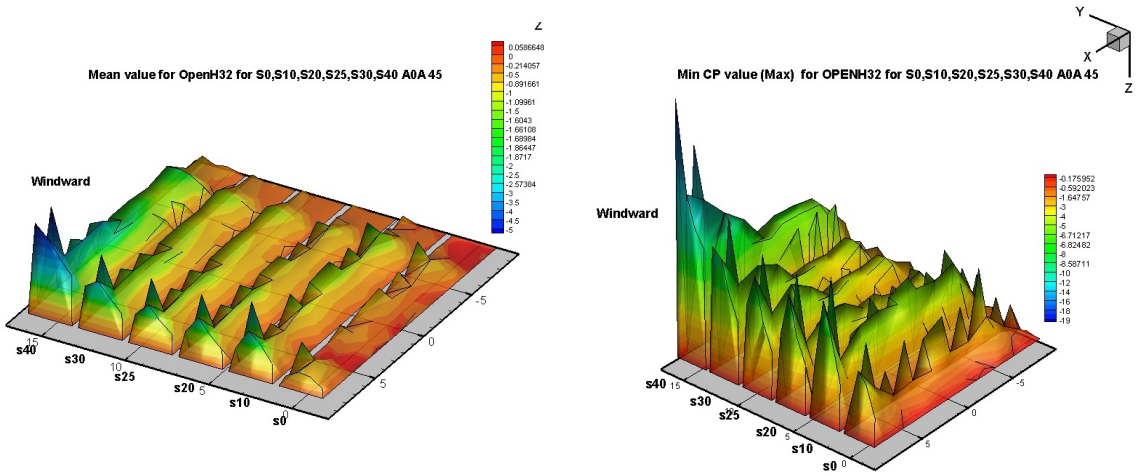

(a) (b)

Figure 21

(a) Mean Cp for S10, S20, S25, S30 and S40 and wind AoA 45^0(open terrain) and (b) maximum Cp for S10, S20, S25, S30 and S40 and wind AoA 45^0.It was clearly shown an increase in the C_p values from the slope 0 to the slope 40.

6.2.4. Effects of upstream exposure (open vs. suburban) on wind pressure coefficients

To study the effects of upstream exposure the worst wind AoAs, 45^0 and 180^0 for a case with support height H=32 in and a slope of 25^0 were considered. Figures 22a and 22b show comparisons between open and suburban maximum and minimum CP value for an AoA of $45^0$and 180^0, respectively.

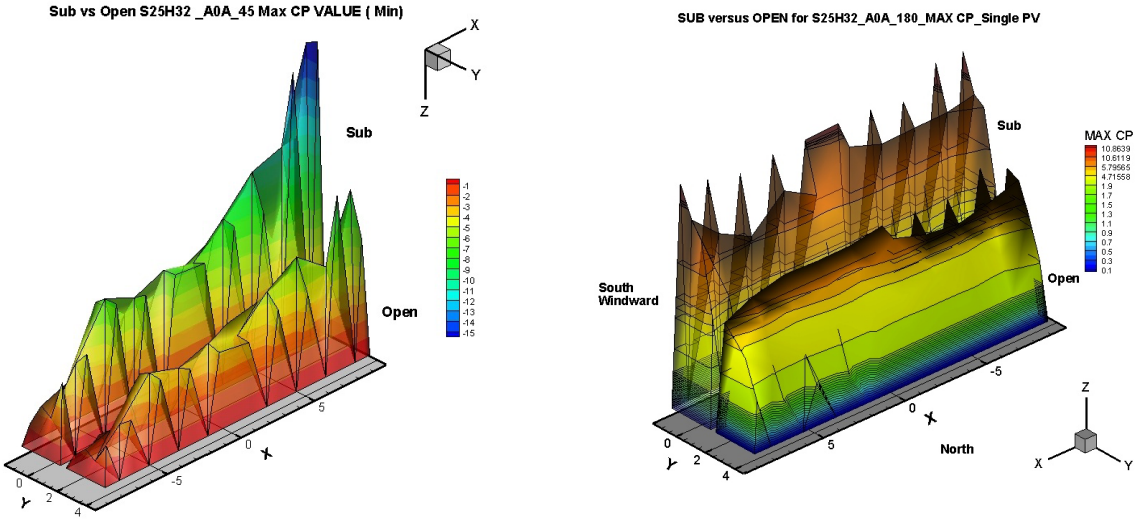

(a) (b)

Figure 22

Variation of the average CP for different open and suburban profiles (a) 45^0 and (b) 180 ^{0} AoA.

Within the figures above the suburban profile shown higher C_P values.

6.3. Solar panel array: study wind tunnel model and instrumentation

6.3.1. Ground- mounted solar pane array

As it has been previously mentioned the data obtained for the *Ground Mounted solar panel arrays* included three variables: (i) the wind direction (AoA), (ii) Longitudinal distance between the solar panel, and (iii) lateral gap between the solar panel.

6.3.1.1. Variation of wind pressure coefficients with wind angle of attack (AOA)

A solar panel with a slope of 25^0, and H = 32in and zero longitudinal distance between the solar arrays was selected to show the variation of the pressure coefficients for four different wind AoA (0^0, 180^0, 225^0 and 315^0). As mentioned before, this slope was selected as it is more representative for South Florida's latitude. Figures 23a, 23b, 23c and 23d show the net C_p contours for wind AOAs 0^0 to AOA 320^0, 220^0 and 180^0.

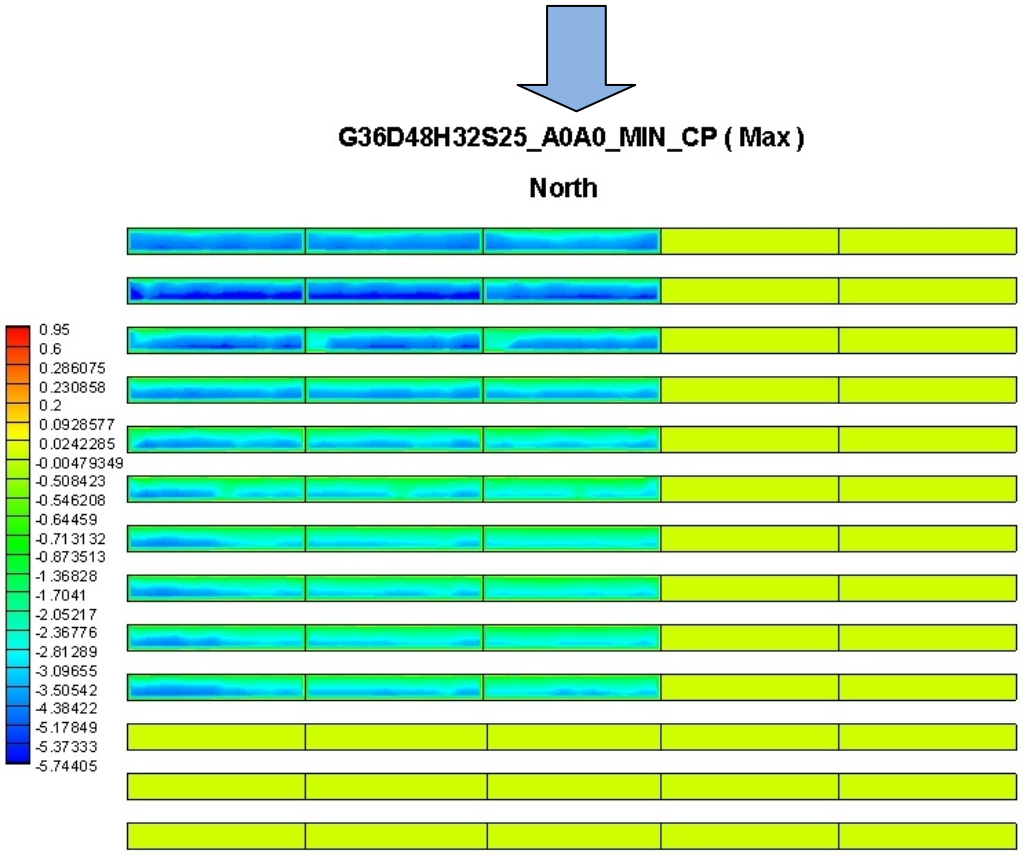
G36D48H32S25_A0A0_MIN_CP (Max)
North
0.95
0.6
0.286075
0.230858
0.2
0.0928577
0.0242285
-0.00479349
-0.508423
-0.546208
-0.64459
-0.713132
-0.873513
-1.36828
-1.7041
-2.05217
-2.36776
-2.81289
-3.09655
-3.50542
-4.38422
-5.17849
-5.37333
-5.74405

(a)

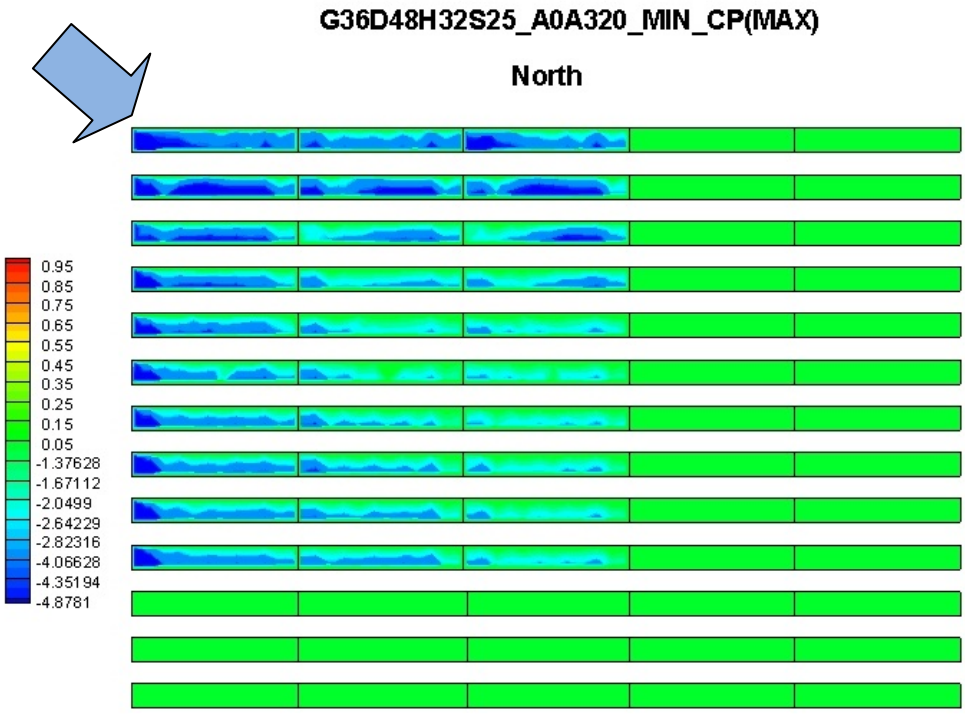
G36D48H32S25_A0A320_MIN_CP(MAX)
North
0.95
0.85
0.75
0.65
0.55
0.45
0.35
0.25
0.15
0.05
-1.37628
-1.67112
-2.0499
-2.64229
-2.82316
-4.06628
-4.35194
-4.8781

(b)

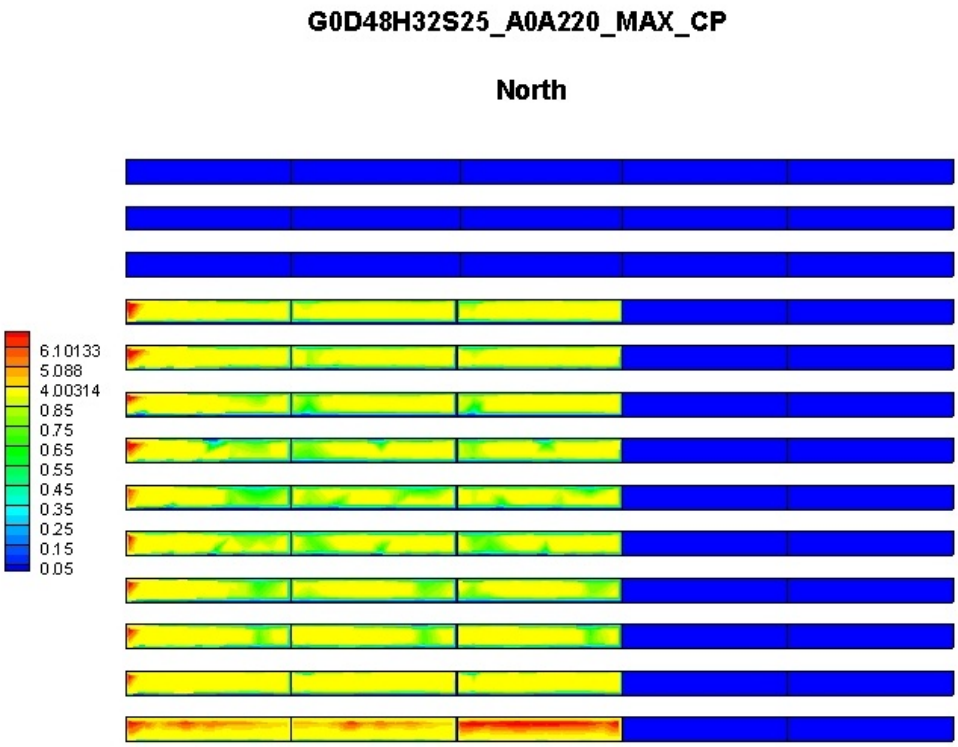
G0D48H32S25_A0A220_MAX_CP
North
6.10133
5.088
4.00314
0.85
0.75
0.65
0.55
0.45
0.35
0.25
0.15
0.05

(c)

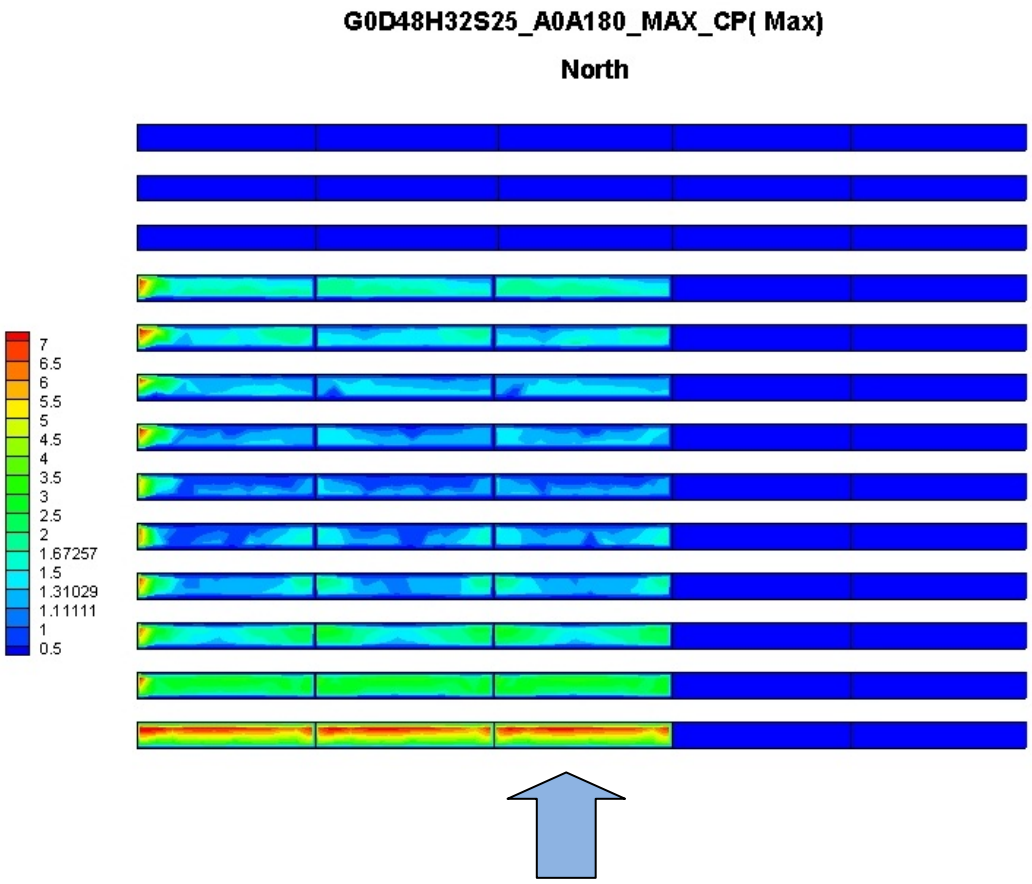

(d)

Figure 23

Net Cp contours for wind AOAs (a) 00 (b) 315^0, (c) 225^0 and (d) 180^0.

6.3.1.2. Effects of longitudinal distance between the arrays on Cp values

A solar panel with a slope of 25^0, and H = 32in was selected to show the effect of longitudinal distance on the pressure coefficients for four different wind AoA (0^0, 180^0, 225^0 and 315^0). Three different longitudinal distances between each panel to represent 24, 48 and 72 inches at full scale were investigated (refer Fig. 7). Figures 24a, 24b, 23c show the net C_p contours for longitudinal gap of 24, 48 and 72

respectively for AoA 0^0. Figures 25a to c show the same C_p contours but for to AOA 315^0. Figures 26a to c show the same C_p contours but for AoA 225^0.From figures 26a to figure c the same C_p contours but for AoA 180^0.

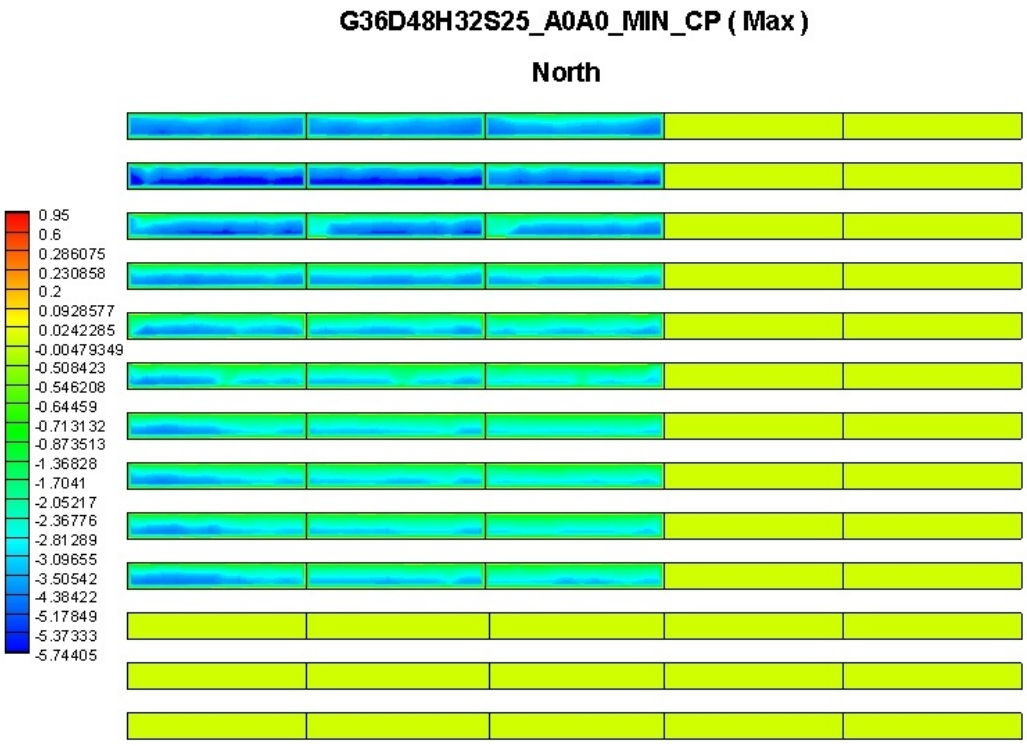

(a)

Figures 24

Ground-mounted arrays: net Cp contours for longitudinal gap (a) 24 in, (b) 48 in and (c) 72 and AoA 0^0.

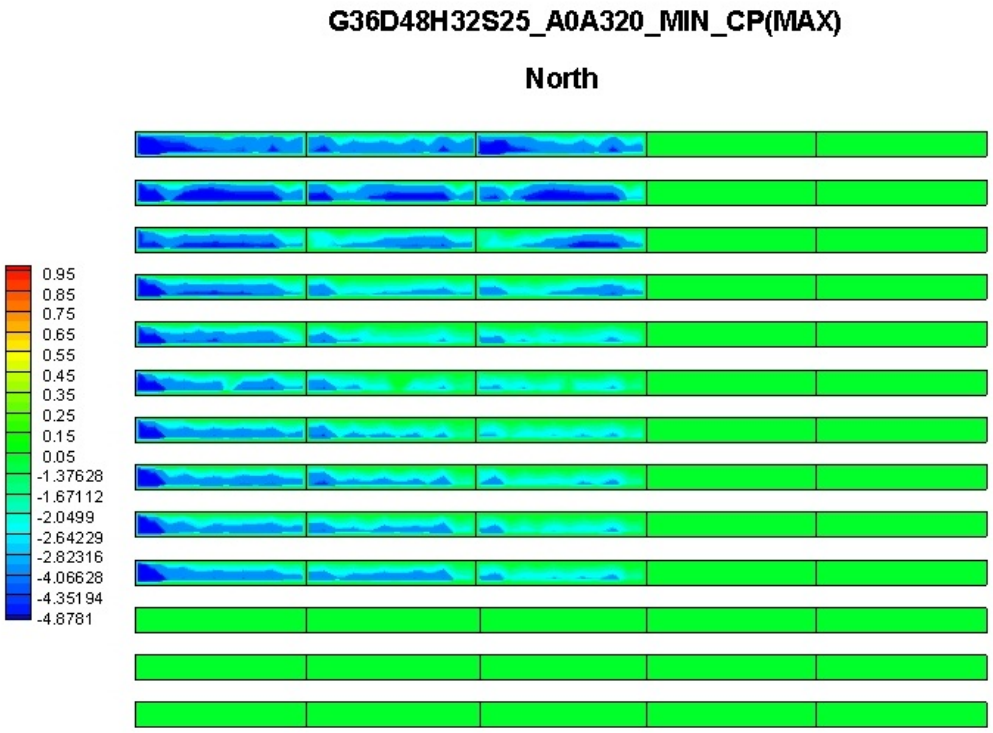

(a)

Figures 25

Ground-mounted arrays: Net Cp contours for longitudinal gap (a) 24 in, (b) 48 in and (c) 72 and AoA 315^0.

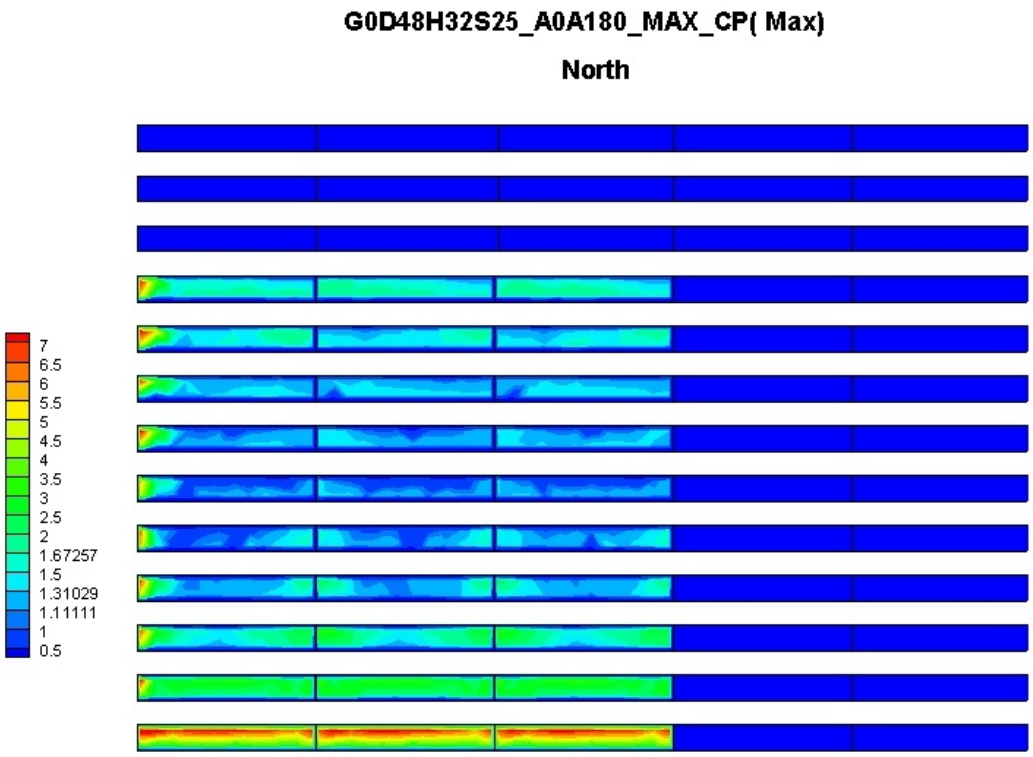

(b)

Figures 26

Ground-mounted arrays: Net Cp contours for longitudinal gap (a) 24 in, (b) 48 in and (c) 72 and AoA 180^0.

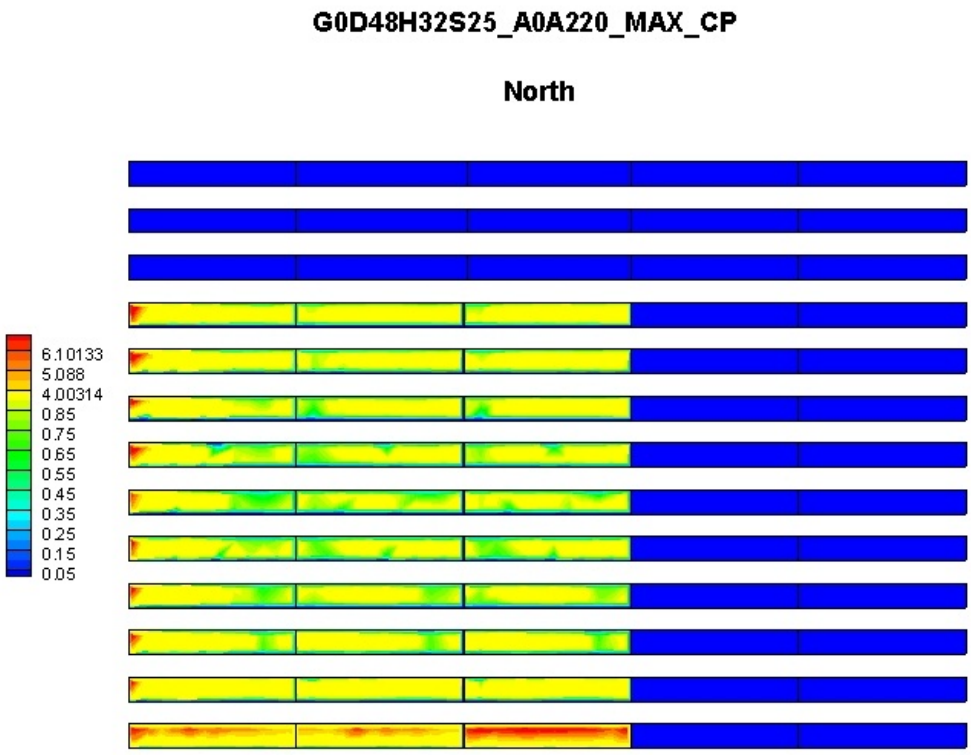

(b)

Figures 27

Ground-mounted array: net Cp contours for longitudinal gap (a) 24 in, (b) 48 in and (c) 72 and AoA 215^0.

6.3.1.3. Effects of Lateral gap between the solar panel on Cp values

A solar panel with a slope of 25^0, and H = 32 in was selected to show the effect of longitudinal distance on the pressure coefficients for four different wind AoA (0^0, 180^0, 225^0 and 315^0). Three different longitudinal distances between each

panel to represent 0, 32 and 72 inches at full scale were investigated (refer Fig. 7). Figures 28a, 28b, 28c show the net Cp contours for lateral gaps of 0, 32 and 72 respectively for AoA 0^0. Figures 29a to c show the same C_p contours but for to AOA 315^0. Figures 30a to c show the same C_p contours but for AoA 225^0. From figure 31(a) to figure (c) the same C_p contours but for AoA 180^0 are shown.

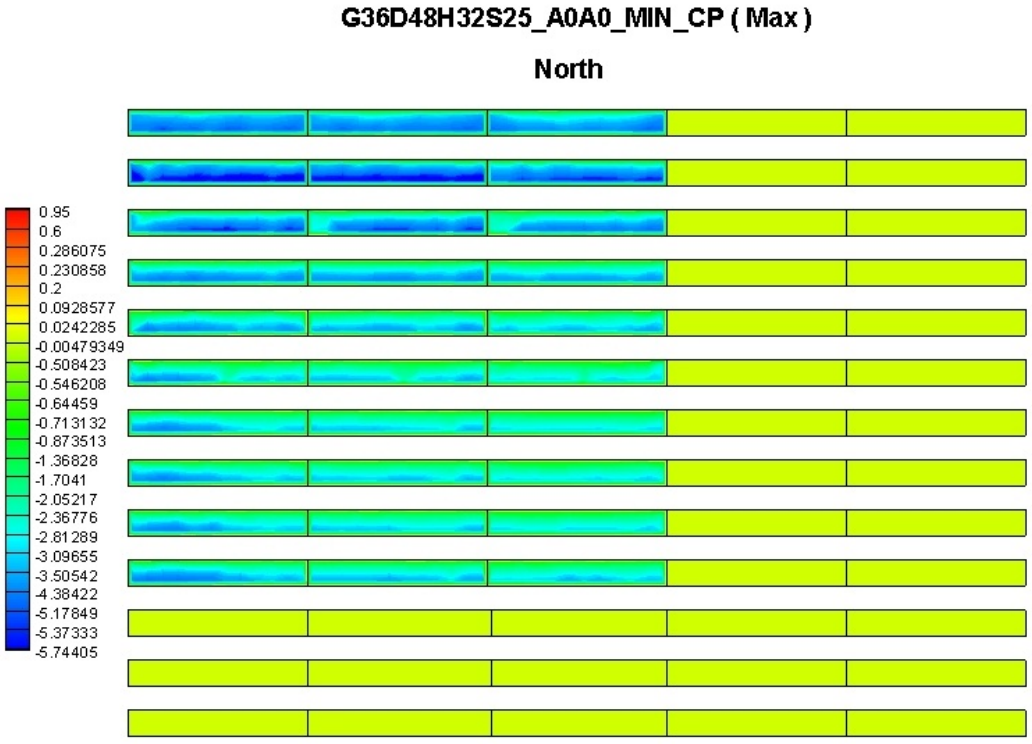

(a)

Figures 28

Ground-mounted array: net Cp contours for lateral gap (a) 0 in, (b) 32 in and (c) 72 and AoA 0^0.

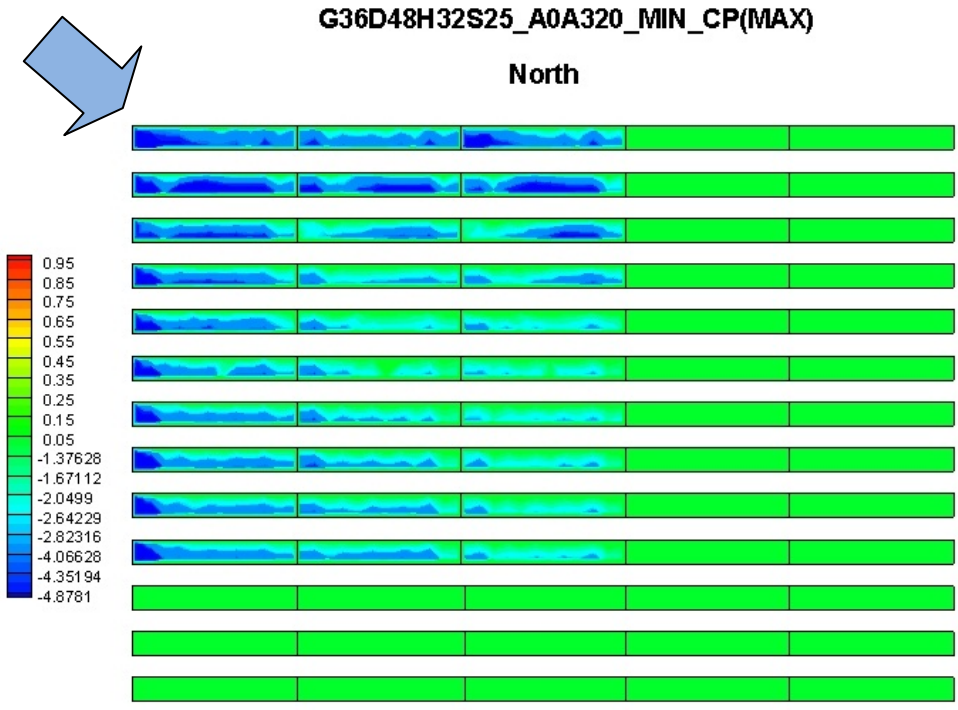

(a)

Figure 29

Ground-mounted array: net Cp contours for lateral gap (a) 0 in, (b) 32 in and (c) 72 and AoA 315^0.

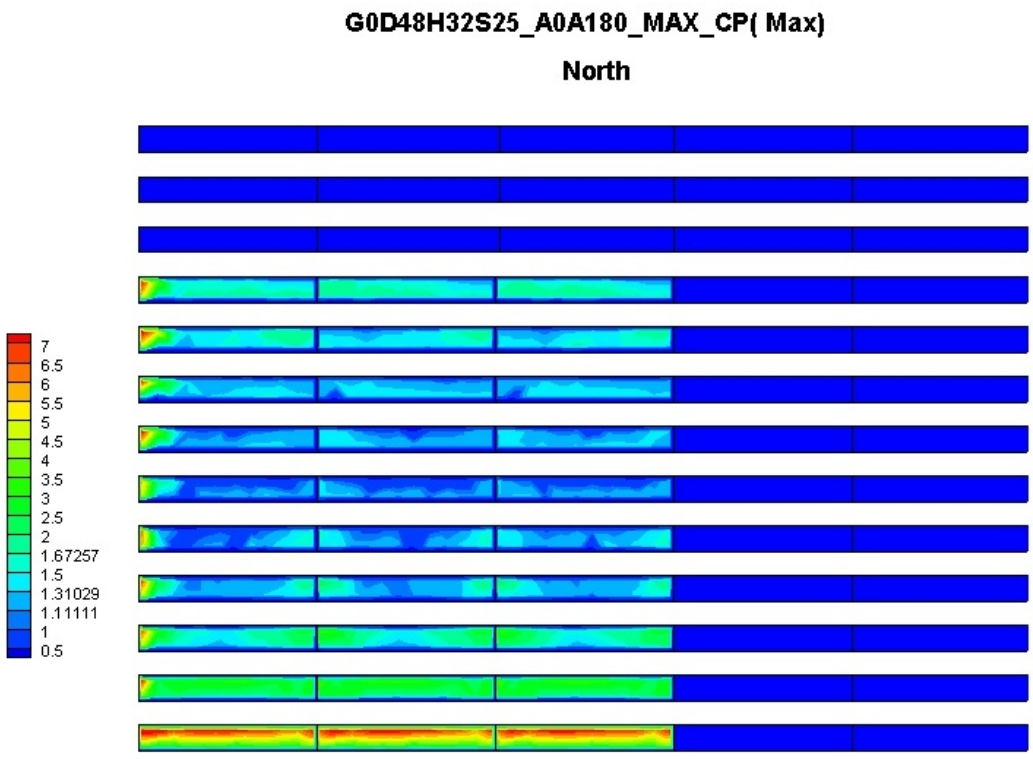

(a)

Figures 30

Ground-mounted array: net Cp contours for lateral gap (a) 0 in, (b) 32 in and (c) 72 and AoA 180^0.

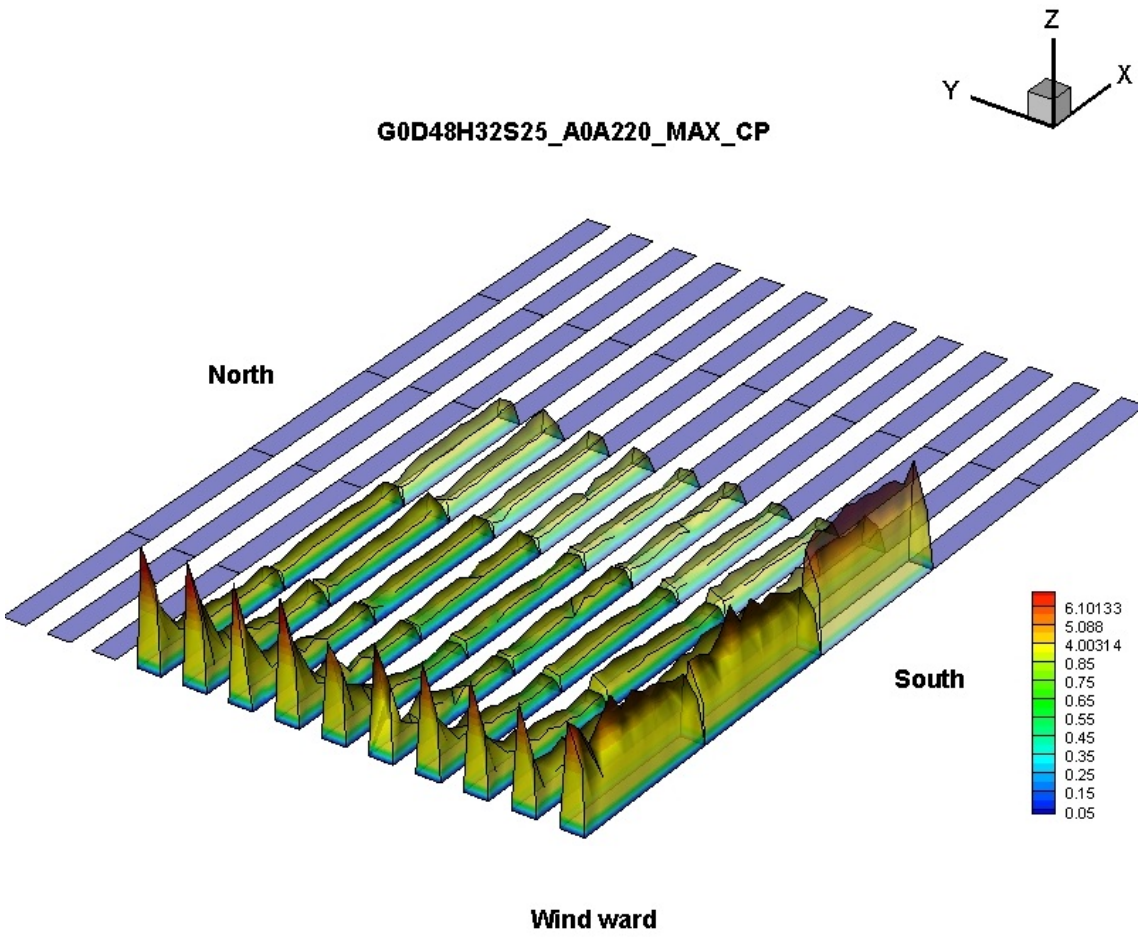
Z
Y
X
G0D48H32S25_A0A220_MAX_CP
North
South
6.10133
5.088
4.00314
0.85
0.75
0.65
0.55
0.45
0.35
0.25
0.15
0.05
Wind ward

(a)

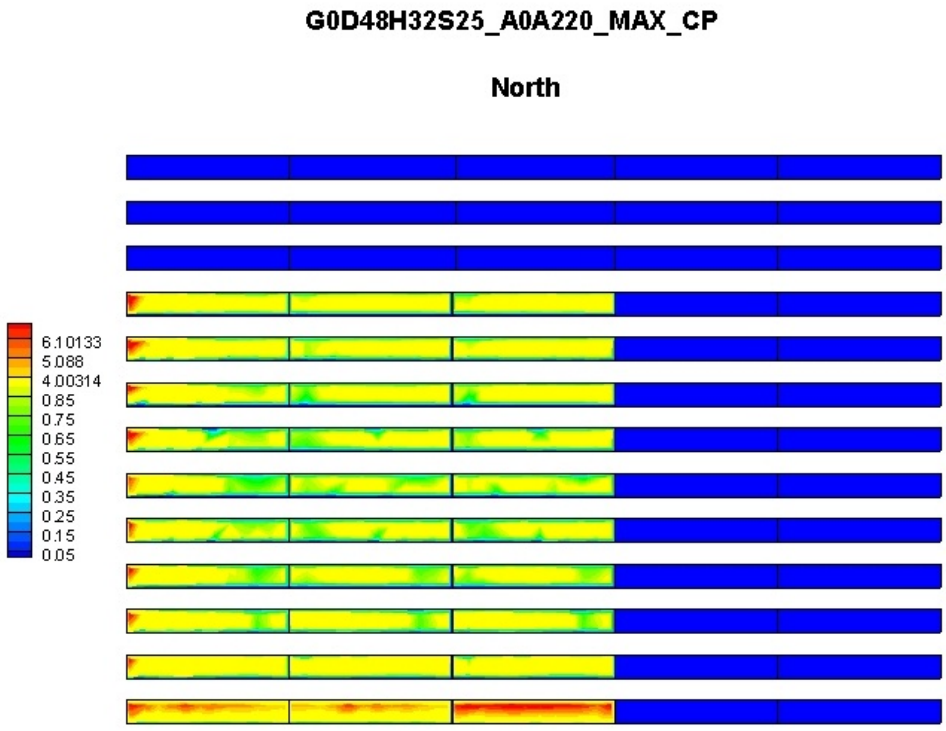

(a)

Figure 31

Ground-mounted arrays: net Cp contours for lateral gap (a) 0 in, (b) 32 in and (c) 72 and AoA 215^0.

6.3.2. Roof Mounted solar panels array

As it has been previously mentioned, the data obtained for the roof-mounted solar panel arrays included two variables: (i) the wind AoA, (ii) roof perimeter gap.

6.3.2.1. Variation of wind pressure coefficients with wind angle of attack (AoA)

A solar panel with a slope of 25^0, and H = 32 in and zero roof perimeter gap was selected to show the variation of the pressure coefficients for four different wind AoA (0^0, 180^0, 225^0 and 315^0).

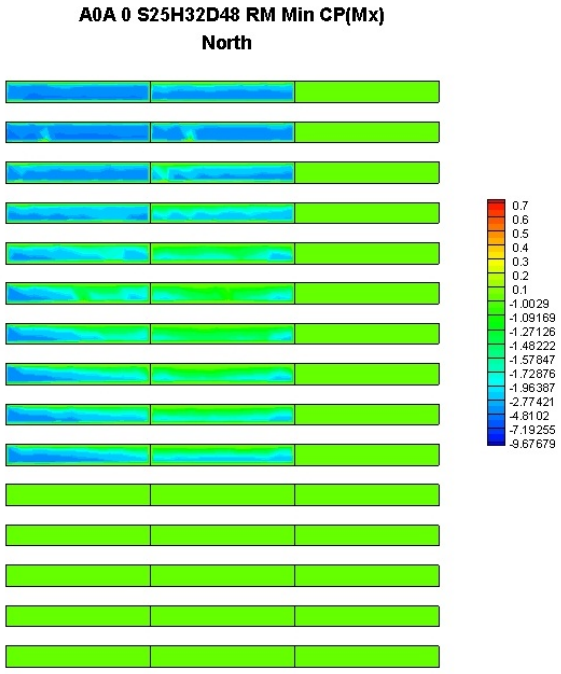

A0A 315 S25H32D48 RM Min CP
North

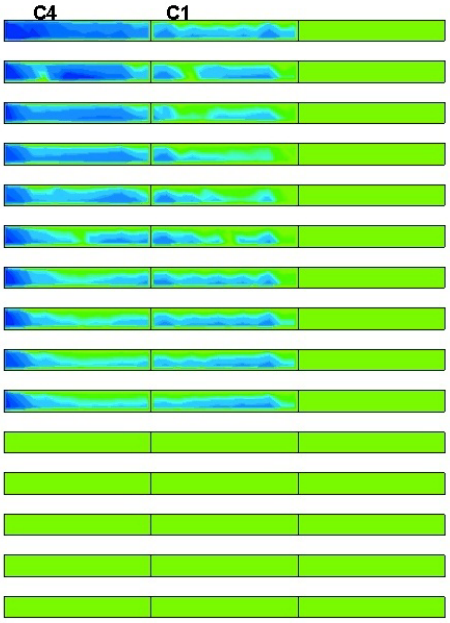

A0A 225 S25H32 MAX CP
North

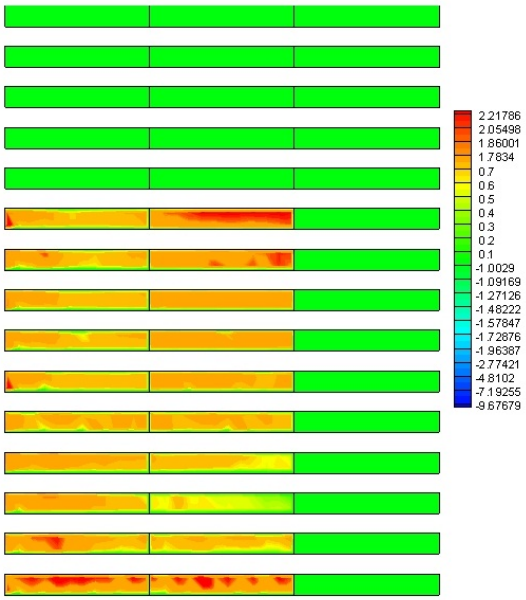

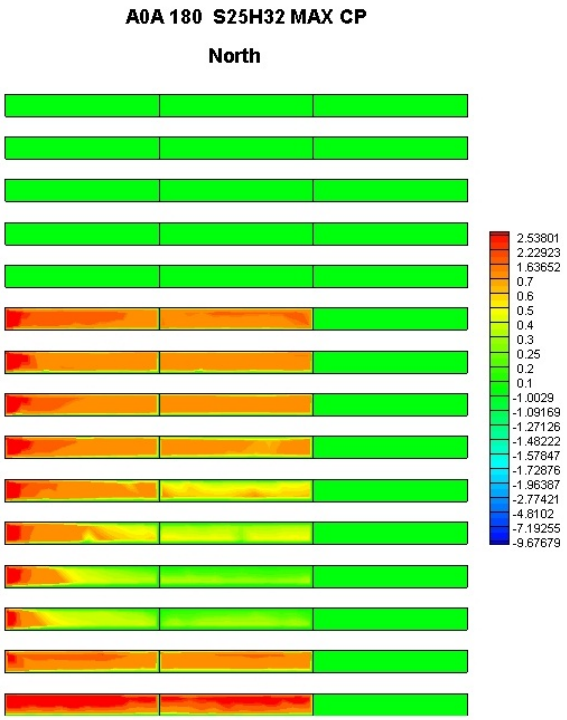

Figure 24

32a, 32b, 32c and 32d show the net Cp contours for wind AOAs 0^0 to AOA 3150, 225^0 and 180^0 and zero perimeter gap.

6.3.2.2. Effects of roof perimeter gap on Cp values

A solar panel with a slope of 25^0, and H = 32 in was selected to show the effect of longitudinal distance on the pressure coefficients for four different wind AoA (0^0, 180^0, 225^0 and 315^0). Three different roof perimeter gaps to represent 0, 36 and 72 inches at full scale were investigated (refer Fig. 7). Figures 33a, 33b, 33c show the net C_p contours for lateral gaps of 0, 36 and 72 respectively for AOA 0^0. Figures 34a to c show the same C_p contours but for to AOA 315^0. Figures 35a to c show the same C_p contours but for AoA 225^0.From figures 36a to figure c the same C_p contours but for AoA 180^0.

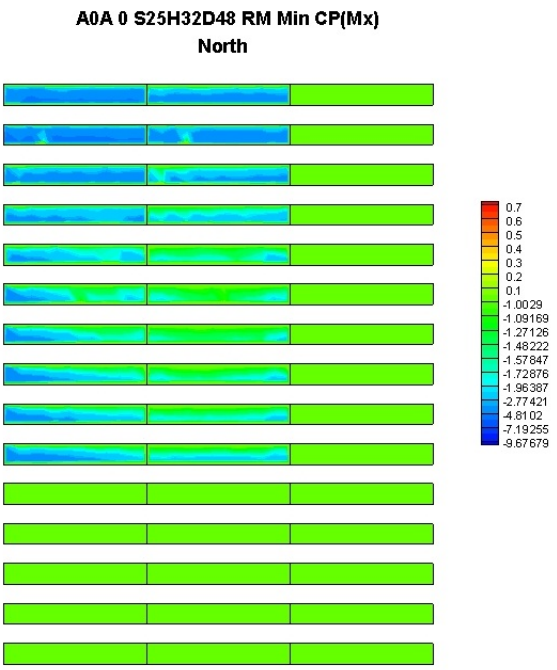
A0A 0 S25H32D48 RM Min CP(Mx)
North
0.7
0.6
0.5
0.4
0.3
0.2
0.1
-1.0029
-1.09169
-1.27126
-1.48222
-1.57847
-1.72876
-1.96387
-2.77421
-4.8102
-7.19255
-9.67679

(a)

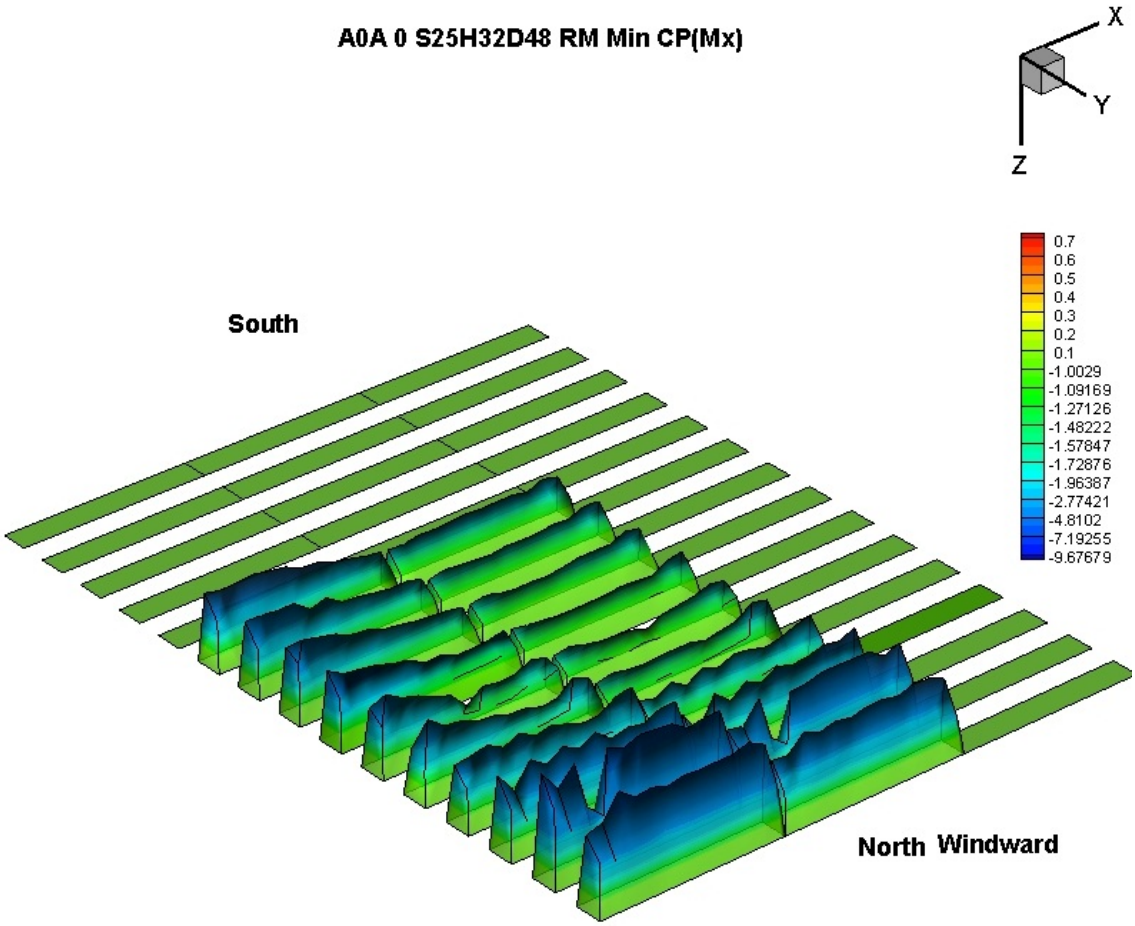
A0A 0 S25H32D48 RM Min CP(Mx)
X
Y
Z
0.7
0.6
0.5
0.4
0.3
0.2
0.1
-1.0029
-1.09169
-1.27126
-1.48222
-1.57847
-1.72876
-1.96387
-2.77421
-4.8102
-7.19255
-9.67679
South
North Windward

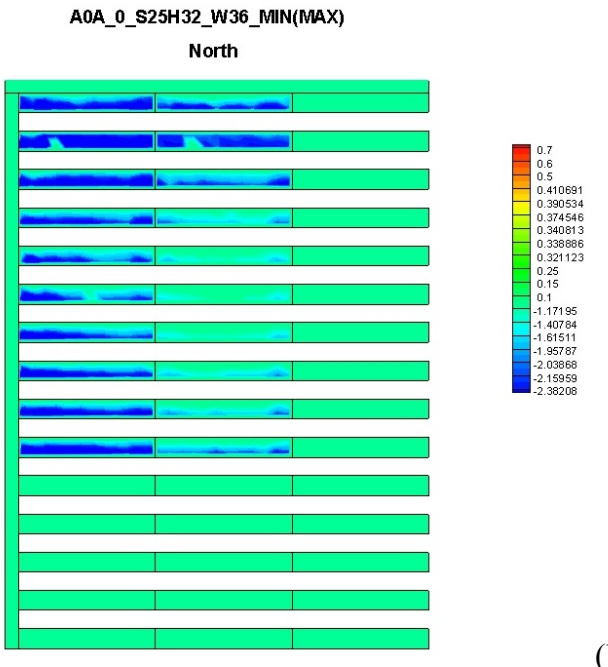
A0A_0_S25H32_W36_MIN(MAX)
North
0.7
0.6
0.5
0.410691
0.390534
0.374546
0.340813
0.338886
0.321123
0.25
0.15
0.1
-1.17195
-1.40784
-1.61511
-1.95787
-2.03868
-2.15959
-2.38208

(b)

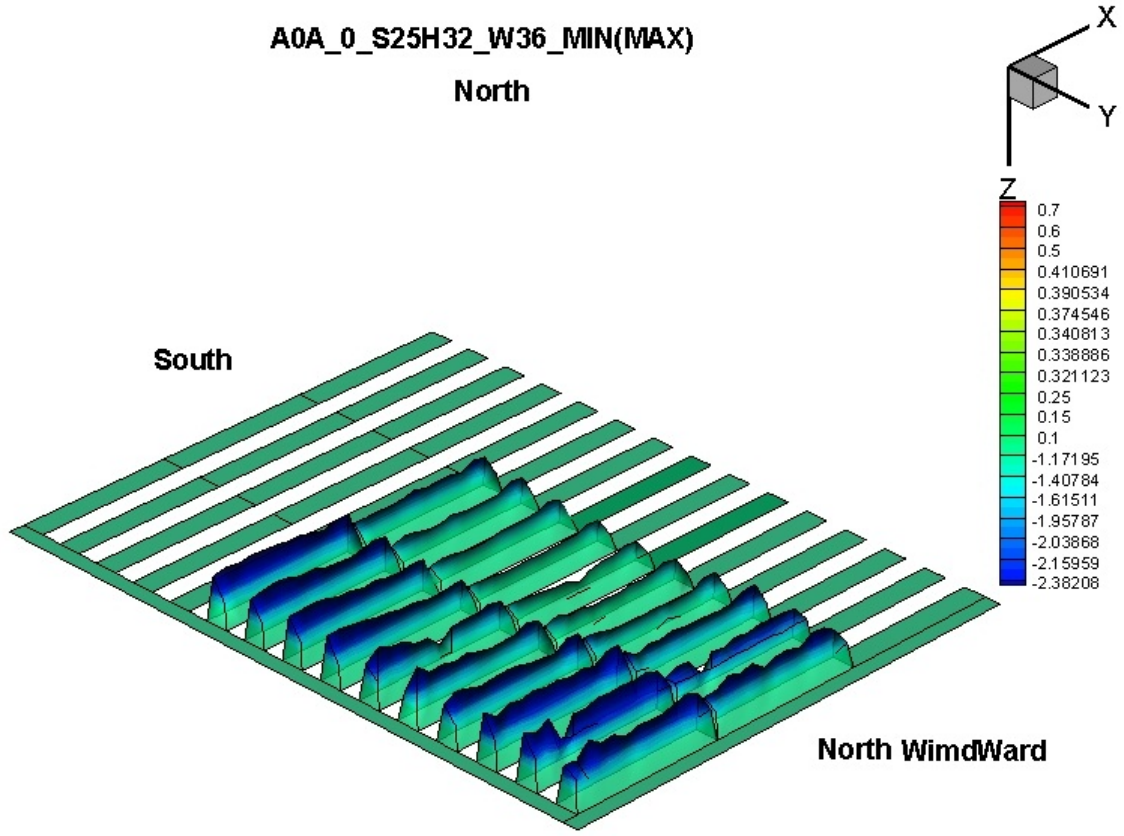
A0A_0_S25H32_W36_MIN(MAX)
North
X
Y
Z
0.7
0.6
0.5
0.410691
0.390534
0.374546
0.340813
0.338886
0.321123
0.25
0.15
0.1
-1.17195
-1.40784
-1.61511
-1.95787
-2.03868
-2.15959
-2.38208
South
North WimdWard

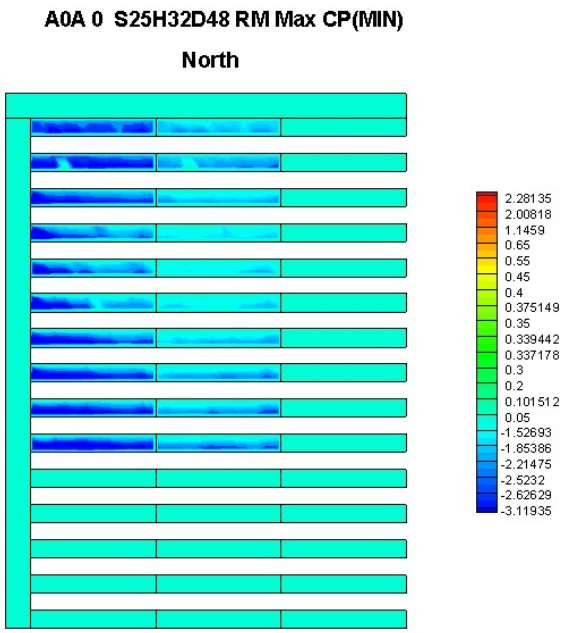

(c)

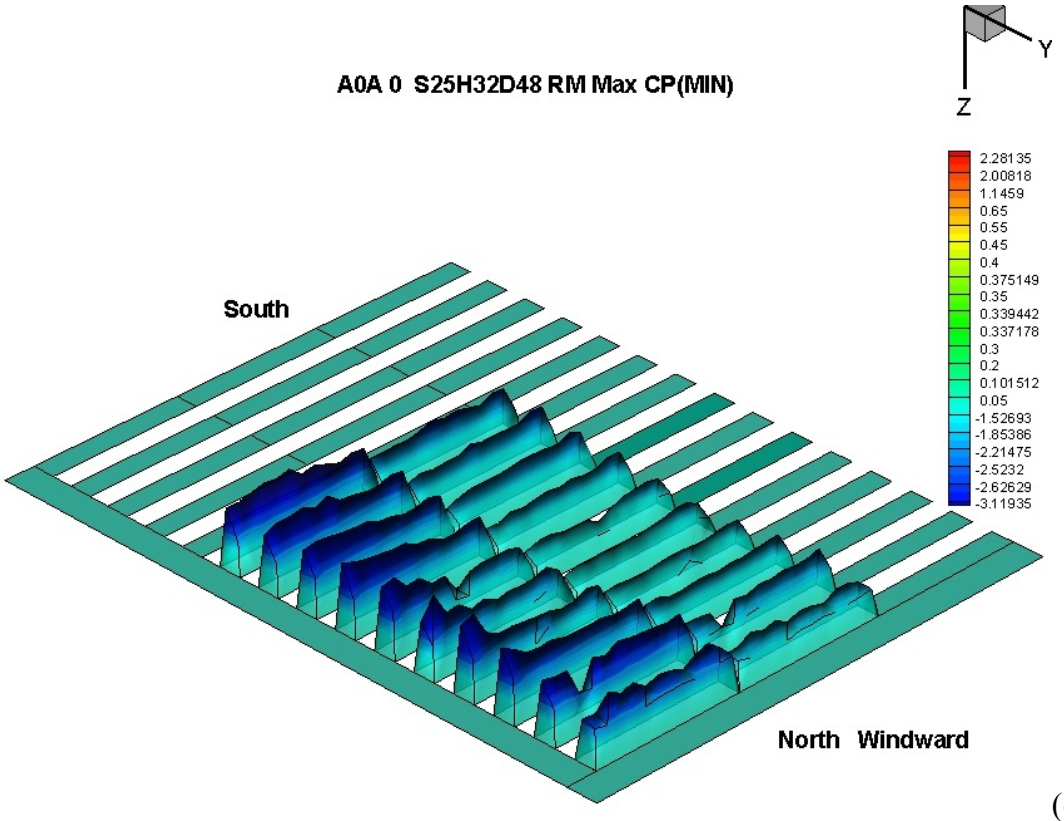

(c)

Figure 33 Roof-mounted arrays: net Cp contours for roof perimeter (a) 0 in, (b) 36 in and (c) 72 and AoA 0^0.

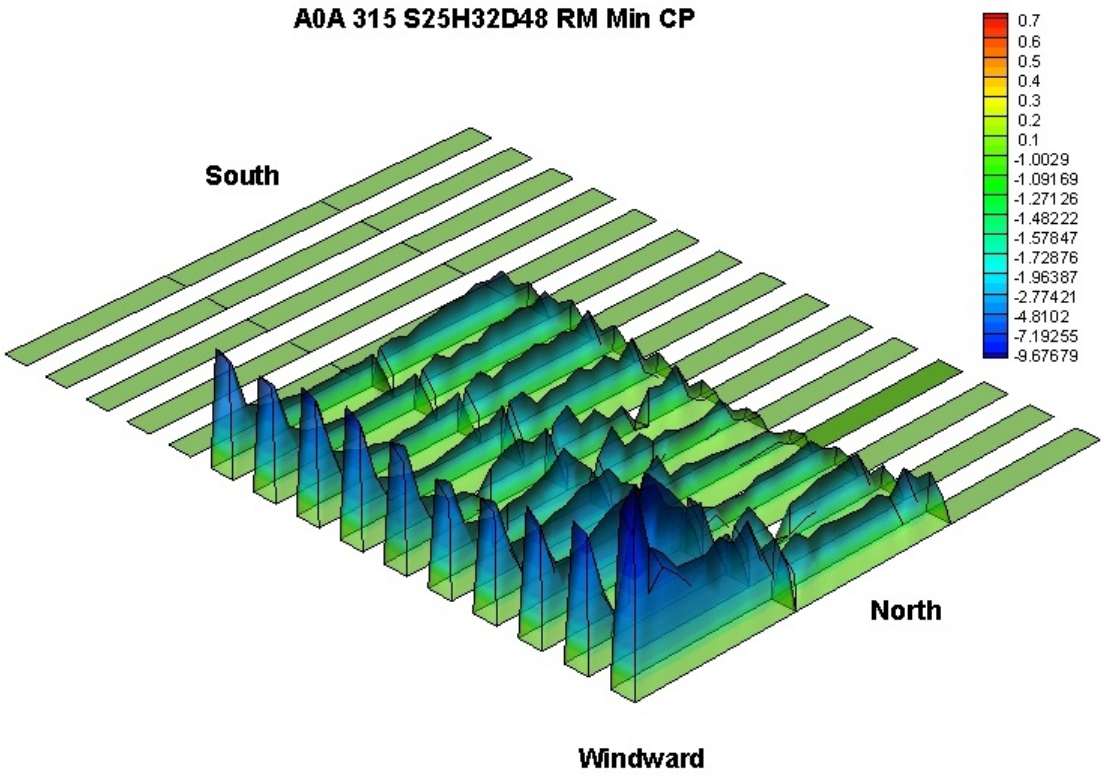
A0A 315 S25H32D48 RM Min CP
South
North
Windward
0.7
0.6
0.5
0.4
0.3
0.2
0.1
-1.0029
-1.09169
-1.27126
-1.48222
-1.57847
-1.72876
-1.96387
-2.77421
-4.8102
-7.19255
-9.67679

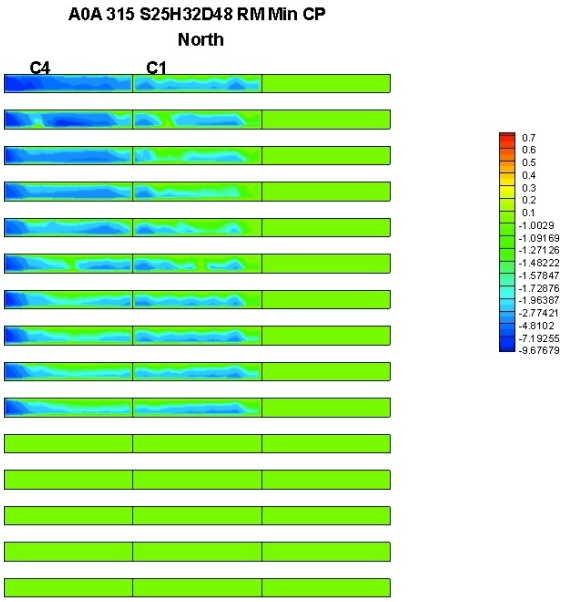
A0A 315 S25H32D48 RM Min CP
North
C4
C1
0.7
0.6
0.5
0.4
0.3
0.2
0.1
-1.0029
-1.09169
-1.27126
-1.48222
-1.57847
-1.72876
-1.96387
-2.77421
-4.8102
-7.19255
-9.67679

a)(a)

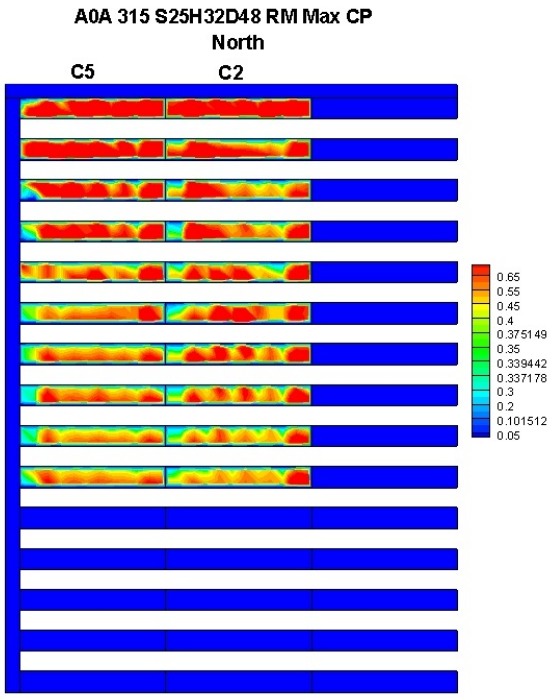

(b)

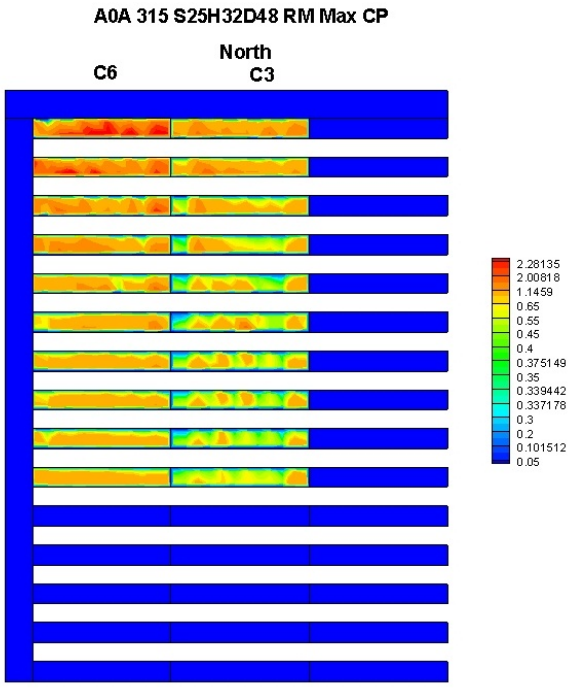

(c)

Figure 34 Roof-mounted arrays: net Cp contours for roof perimeter (a) 0 in, (b) 36 in and (c) 72 and AoA 315^0.

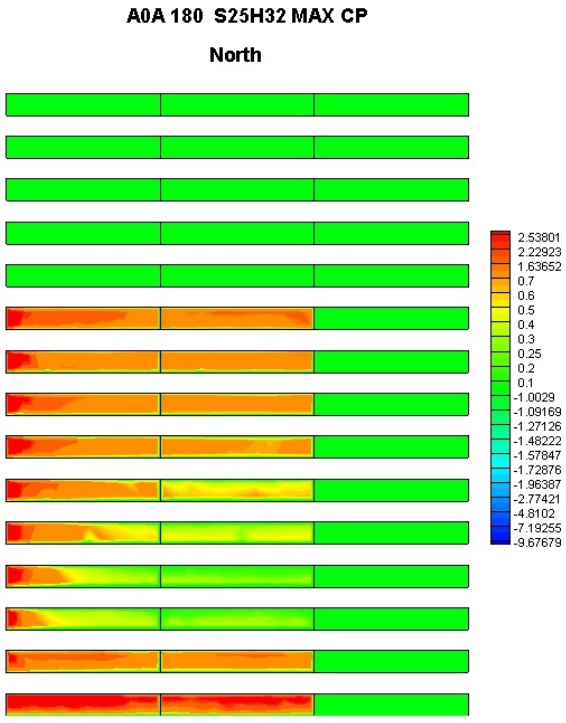

(a)

Figure 35

Roof-mounted arrays: net Cp contours for roof perimeter (a) 0 in, (b) 36 in and (c) 72 and AoA 180^0.

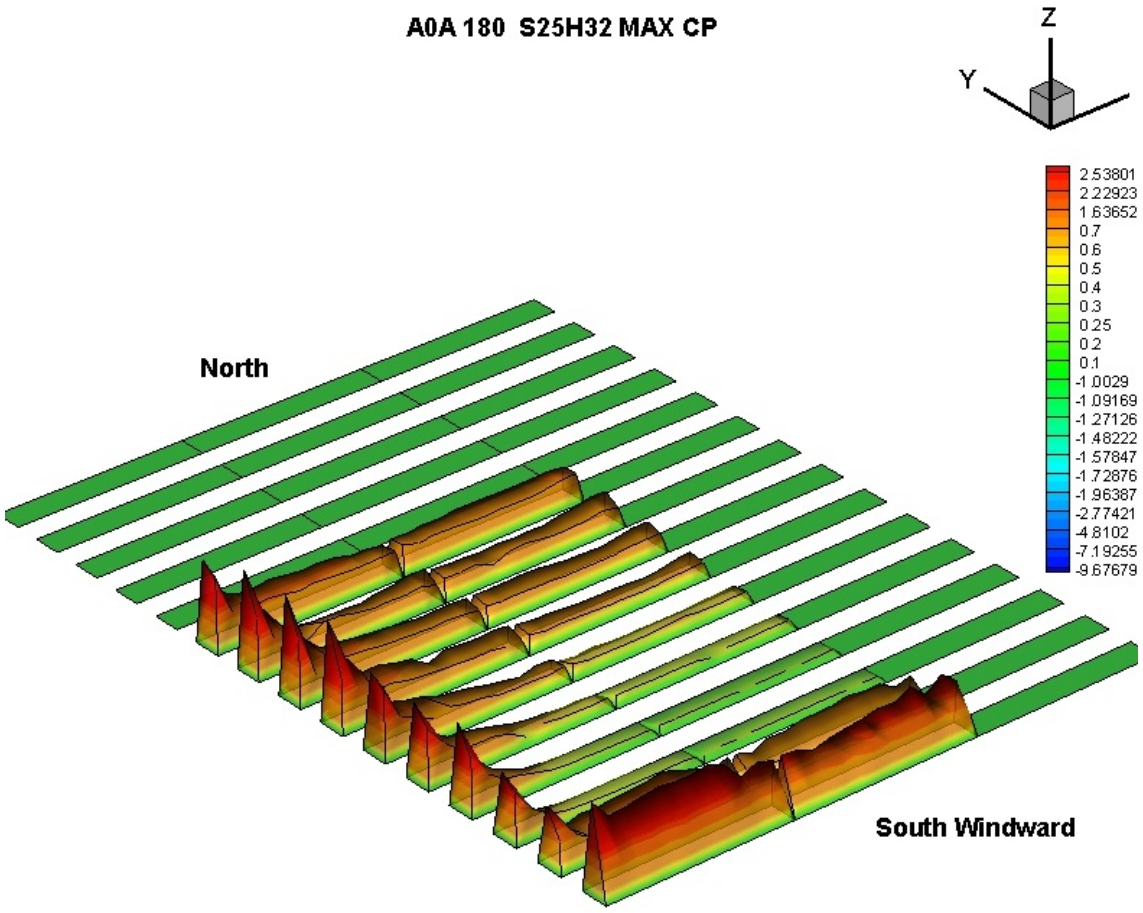
A0A 180 S25H32 MAX CP
Z
Y
2.53801
2.22923
1.63652
0.7
0.6
0.5
0.4
0.3
0.25
0.2
0.1
-1.0029
-1.09169
-1.27126
-1.48222
-1.57847
-1.72876
-1.96387
-2.77421
-4.8102
-7.19255
-9.67679
North
South Windward

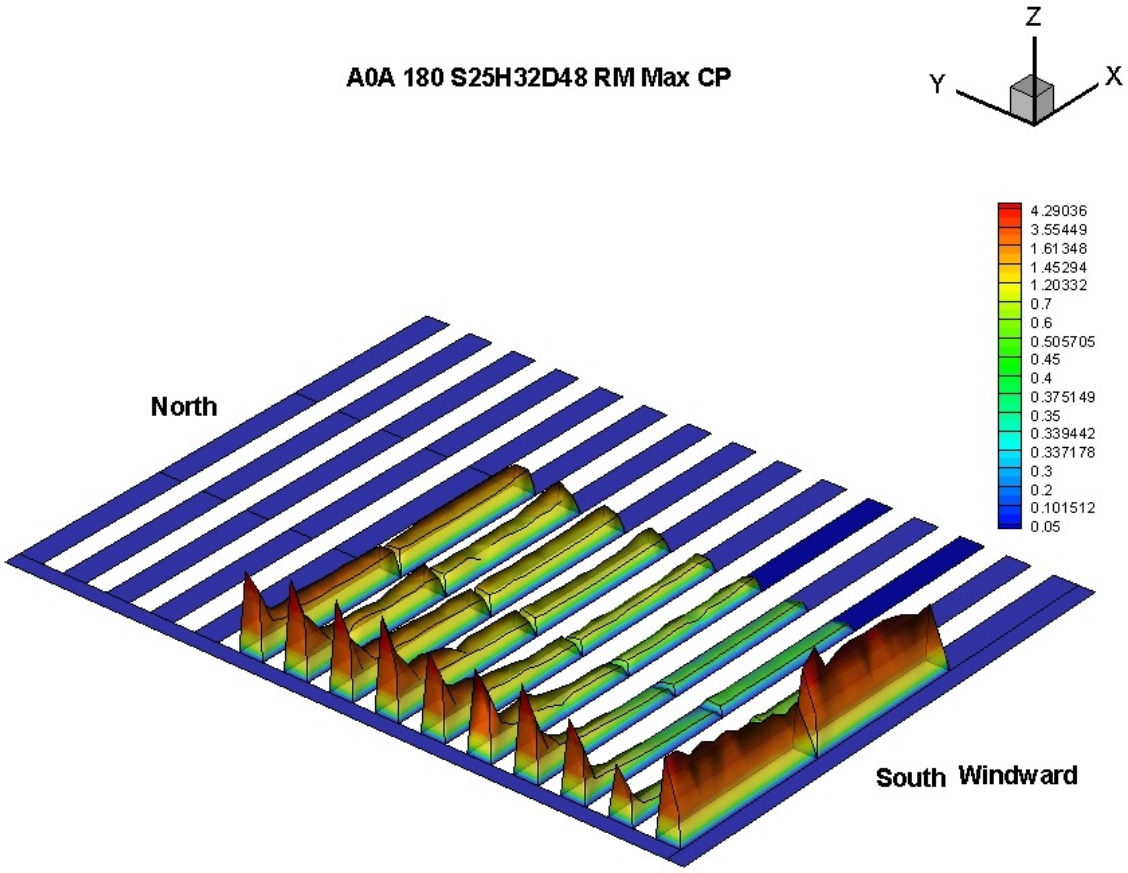
A0A 180 S25H32D48 RM Max CP
Z
Y
X
4.29036
3.55449
1.61348
1.45294
1.20332
0.7
0.6
0.505705
0.45
0.4
0.375149
0.35
0.339442
0.337178
0.3
0.2
0.101512
0.05
North
South
Windward

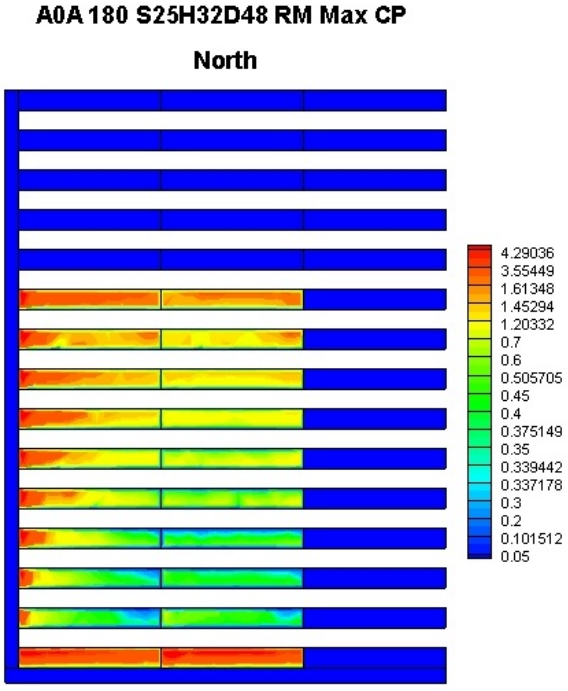
A0A 180 S25H32D48 RM Max CP
North
4.29036
3.55449
1.61348
1.45294
1.20332
0.7
0.6
0.505705
0.45
0.4
0.375149
0.35
0.339442
0.337178
0.3
0.2
0.101512
0.05

(b)

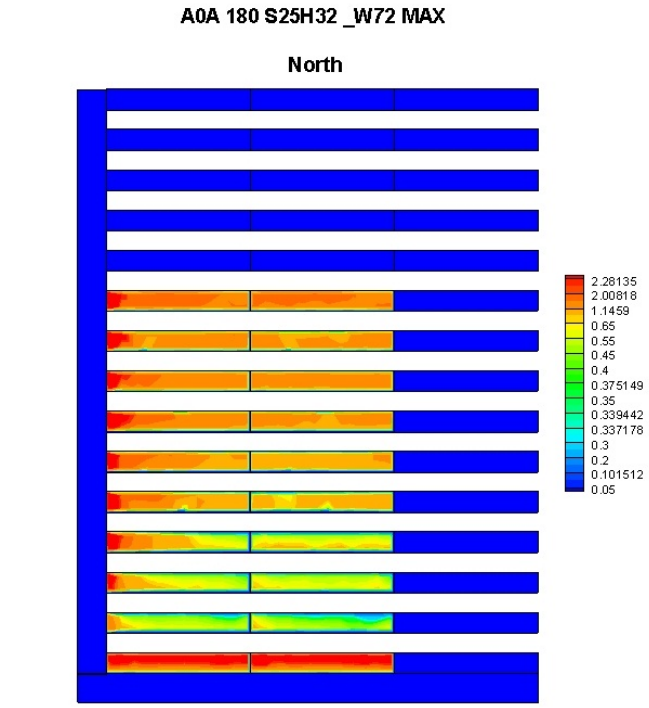
A0A 180 S25H32 _W72 MAX
North
2.28135
2.00818
1.1459
0.65
0.55
0.45
0.4
0.375149
0.35
0.339442
0.337178
0.3
0.2
0.101512
0.05

(c)

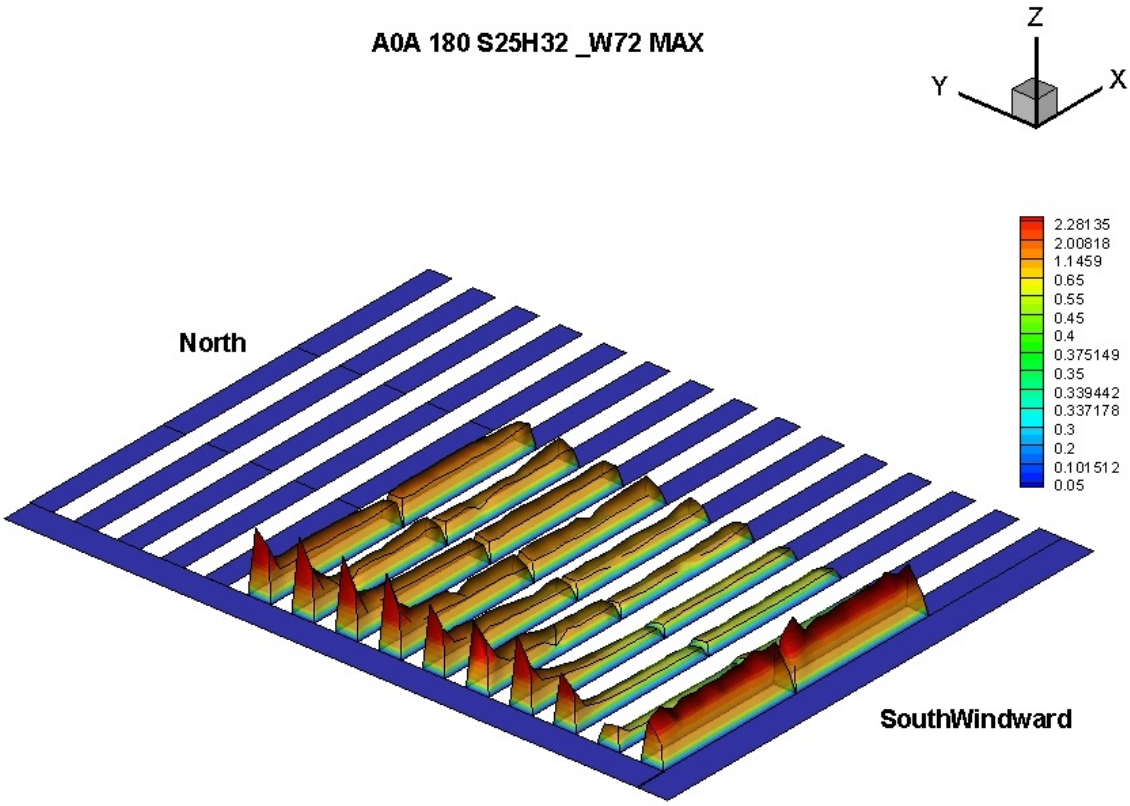
A0A 180 S25H32 _W72 MAX
Z
Y
X
North
2.28135
2.00818
1.1459
0.65
0.55
0.45
0.4
0.375149
0.35
0.339442
0.337178
0.3
0.2
0.101512
0.05
SouthWindward

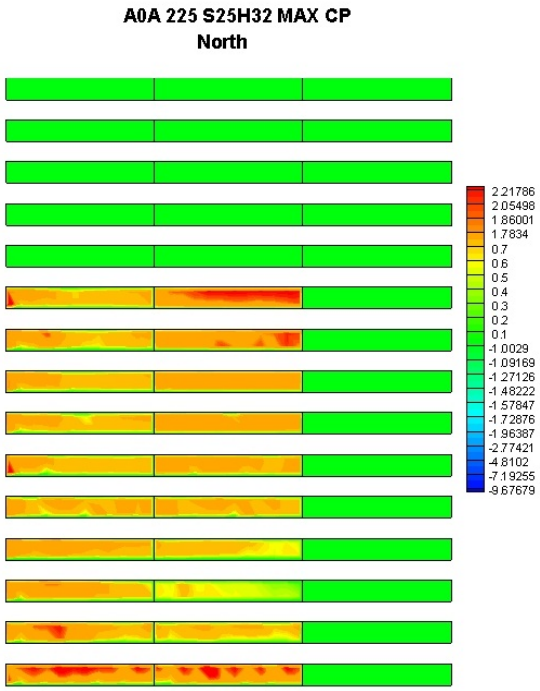

(a)

Figures 36

Roof-mounted arrays: net Cp contours for roof perimeter (a) 0 in, (b) 36 in and (c) 72 and AoA 215^0.

CONCLUSIONS AND RECOMMENDATIONS

By using Boundary Layer Wind Tunnel testing techniques, the present study evaluates the effects of wind on solar panels, and provides explicit and reliable information on design wind loads in the forms of pressure coefficient value. The study considered both, two different types of solar panels arrangements, isolated solar panel and arrays, and two different mounting locations, ground mounted and roof mounted. Detailed design wind load

information was produced as part of this study for isolated and arrayed solar panels. Some of the observations include the following:

For isolated solar panels, the wind load on high sloped ones for wind AoA perpendicular to the main axis exhibited the largest wind loads. For arrays, while the outer rows and column were subjected to high wind loads for AoA perpendicular to the main axis, the interior solar panels were subjected to higher loads for oblique AoA.

For the isolated solar panels a major variations were found in C_p values as a result of both, the different AoA, and different slopes of the panel. A considerable variation in the C_p values was also observed as a result of the solar panel terrain exposure. However no major variation was found as a result of the solar panel support height.

For the ground mounted arrays, the solar panels major variations were found in C_p values as a result of the different AoA. A considerable variation in the C_p values was also observed as a result of both; the longitudinal distance between the arrays, and the lateral gap between the solar panels.

For the roof mounted arrays, the solar panels major variations were found in C_p values as a result of the different AoA. A considerable variation in the C_p values was also observed as a result of the perimeter gap around the solar panels.

REFERENCES

1. Florida Energy facts. Data Sources: Real GDP per capita 2008, Bureau of Economic Analysis.News Release: GDP by State.2009.

2. Chevalien, L., Norton, J. (1979). Wind loads on solar collector panels and support structure. Aerospace Engineering Department, Texas A&M University.

3. Kopp. G.A, Surry. D, Chen. K. (2002). Wind loads on solar array. *Wind and Structures* 5, 393-406.

4. Chung, K., Chang, K., Liu, Y. (2008). Reduction of wind uplift of a solar collector model. *Journal of Wind Engineering and Industrial Aerodynamics* 96, 1294-1306.

5. Alexander Bronkhorst, Jörg Franke, Chris Geurts, Carine van Bentum François Grepinet. (2010).Wind tunnel and CFD modeling of wind pressures on solar energy systems on flat roofs. *The Fifth International Symposium on Computational Wind Engineering* (CWE2010) Chapel Hill, North Carolina, USA May 23-27.

6. Barkaszi & O'Brien (2010).Wind loads calculation for solar panels arrays.2010. *Journal of Wind Engineering and Industrial Aerodynamics* 97, 1294-1306

7. Girma T. Bitsuamlak, Agerneh K. Dagnew, James Erwin. (2010).Evaluation of wind loads on solar panel modules using CFD. *The Fifth International Symposium on Computational Wind* Engineering (CWE2010) Chapel Hill, North Carolina, USA May 23-27.

8. Kopp. G.A, Surry. D, Chen. K. (2002). Wind loads on solar array. *Wind and Structures* Vol. 5, 393-406.

9. Murakami, S., Mochida, A. (1988). 3-D numerical simulation of airflow around a cubic model by means of the model. *Journal of Wind Engineering and Industrial Aerodynamics* 31, 283-303.

10. Nozu, T., Tamura, T., Okuda, Y., Sanada, S. (2008). LES of the flow and building wall pressures in the center of Tokyo. *Journal of Wind Engineering and Industrial Aerodynamics* 96, 1762-1773.

11. Shademan, M., Hangan, H. (2009). Wind Loading on Solar Panels at Different inclination Angles. *The 11th American conference on Wind Engineering. San Juan, Puerto Rico.*

12. Stathopoulos, T. (1997). Computational wind engineering: Past achievements and future challenges. *Journal of Wind Engineering and Industrial Aerodynamics* 67-68, 509-532.

13. Tamura, T., Nozawa, K., Kondo, K. (2008). AIJ guide for numerical prediction of wind loads on buildings. *Journal of Wind Engineering and Industrial Aerodynamics* 96. 1974-1984.

14. Tominaga, Y., Mochida, A., Murakami, S., Sawaki, S. (2008). Comparison of various revised k–ε models and LES applied to flow around a high-rise building model with 1:1:2 shape placed within the surface boundary layer. *Journal of Wind Engineering and Industrial Aerodynamics* 96, 389-411.

15. Florida Building Code. (2007). *Published by Florida Building Commission.*

16. Banks David. (2008). How to Calculate Wind Loads on Roof Mounted Solar Panels in the US. CCP Inc. *Wind Loads and Effects Papers*. 389-411.

17. Geurts Chris P.W, Van Bentum Carine A. (2008) Wind Loads on Solar Energy Roofs. *Eur-Active RooFer Project.*

18. Geurts Chris P.W, Van Bentum Carine A. (2005) Local Wind Loads on Roof Mounted Solar Energy Systems. *Paper presented at 4EACWE, Prague*.

19. Westin Jonas. (2011) Wind Action on Flat-Roof-Mounted Photovoltaic Panels: A Comparison of Design Guidelines. *Lund Institute of Technology, Sweden.*

20. Florida Building Code 2007 with 2009 supplements. *Published by Florida Building Commission.*

21. The 2010 Florida Statutes. Chapter 553 Building Construction Standards, Section 553.73 Florida Building Code. Florida Legislature.

22. Gevorkian Peter. Solar Power in Building Design (2008). The engineer's complete design resource. *The McGraw-Hills Companies, Inc.*

23. Wurfel Peter. (2008). Physics of Solar Cells: From Principles to New Concepts. *Wiley-VCH Co. Hoboken, NJ, USA.*

24. Nelson Jenny. (2003).The Physics of Solar Cells. Imperial College Press. London, UK.

25. Florida Solar Energy Center (FSEC), a research institute of the University of Central Florida.

26. Dyrbye Claèes. (1997). Wind Loads on Structures. *John Wiley & Sons, Inc. England.*

27. Whole Building Design Guide. National Institute of Building Science. Washington, CD. USA.